

**EXAMINATION OF APPROXIMATION ERROR
IN THE FAST MULTIPOLE METHOD**

By

NITA NAGDEWATE

B.S., Government Engineering College, Chandrapur, India

SUBMITTED IN PARTIAL FULFILLMENT OF THE REQUIREMENTS
FOR THE DEGREE OF MASTERS OF SCIENCE
IN ELECTRICAL ENGINEERING
UNIVERSITY OF MASSACHUSETTS LOWELL

Signature of Author: Date:

Signature of Thesis Supervisor:

Charles Thompson, Ph.D, Professor

Signature of Other Thesis Committee Members:

.....

Kavitha Chandra, Eng.D, Professor

.....

Max Denis, Ph.D, Research Fellow at Mayo Clinic

**EXAMINATION OF APPROXIMATION ERROR
IN THE FAST MULTIPOLE METHOD**

By

NITA NAGDEWATE

ABSTRACT OF A THESIS SUBMITTED TO THE FACULTY OF THE
DEPARTMENT OF ELECTRICAL AND COMPUTER ENGINEERING
IN PARTIAL FULFILLMENT OF THE REQUIREMENTS
FOR THE DEGREE OF MASTER OF SCIENCE
UNIVERSITY OF MASSACHUSETTS LOWELL
2015

Thesis Supervisor: Charles Thompson, Ph.D

Professor, Department of Electrical and Computer Engineering

ABSTRACT

In this thesis, a single layer implementation of the fast multipole method for the solution of the three dimensional Helmholtz equation is developed. The cartesian and spherical harmonic representations of the free-space Green's function is derived and the Kirchhoff integral formulation of the solution to the Helmholtz equation is presented. Error analyzes are undertaken for single and multipole cases. It is shown that translation errors can be problematic if the distance between subdomain centers is less than a wavelength.

ACKNOWLEDGMENTS

I would like to thank my advisor Professor Charles Thompson. I sincerely appreciate his guidance, motivation, and support. I would like to thank Professor Kavitha Chandra for her guidance and motivation. I would also like to thank Dr. Max Denis for serving on my committee. I am thankful for their support as thesis committee members. I appreciate the help and support from my colleagues at the Center for Advanced Computation and Telecommunications. I am thankful to my friends and family for always being there as a support.

TABLE OF CONTENTS

LIST OF FIGURES	ix
LIST OF NOMENCLATURE	ix
0.1 Background	1
0.2 Objective	2
0.3 Organization of the Thesis	3
1 SOLUTION TO THE HELMHOLTZ EQUATION	4
1.1 Introduction	4
1.2 Solution of the Helmholtz Equation in Cartesian Coordinates	4
1.3 Green's Function for the Helmholtz Equation in terms of Spherical Harmonics	10
1.4 Approximation Error	17
1.5 Kirchhoff Integral Formula	21
2 ERROR ANALYSIS FOR THE GREEN'S FUNCTION AND THE EXPAN- SION COEFFICIENT	23
2.1 Introduction	23

2.2	Multipole expansion	24
2.3	the FMM Evaluation of the Kirchhoff Integral	26
2.4	Multipole Expansion about an Arbitrary Reference Point	29
2.5	Numerical Results for the Accuracy of the Potential with the Expansion Coefficients	32
2.5.1	Accuracy for the Green's function	32
2.5.2	Approximation Error for the Potential with the Expansion Coefficients	34
3	TRANSLATION ERROR ANALYSIS FOR SINGLE LEVEL FAST MULTIPOLE METHOD(SLFMM)	36
3.1	Introduction	36
3.2	Translation Coefficients	36
3.3	Translation Error Analysis for the Green's Function	41
3.4	Translation Error analysis for the cubically shaped subdomains . . .	43
3.5	Hankel function and Divergence of the Green's function	47
3.6	Translation Error analysis for the spherically shaped subdomains . .	49
3.7	Conclusion	51
	Appendices	52
1	DERIVATION OF THE SOLUTION TO THE HELMHOLTZ WAVE EQUATION IN SPHERICAL COORDINATE SYSTEM	53
2	VARIETY OF SPECIAL FUNCTIONS	56

2.0.1	Bessel Functions	56
2.0.2	Legendre Functions and Polynomials	58
2.0.3	Spherical Harmonics	59
BIBLIOGRAPHY		60

LIST OF FIGURES

Figure

1.1	Contour integral	6
1.2	Spherical coordinate system	10
1.3	Regular and singular solutions for $ \vec{r} > \vec{r}_0 $	16
1.4	Regular and singular solutions for $ \vec{r} < \vec{r}_0 $	16
1.5	Approximation error for $T = 16$	19
1.6	Approximation error for $T = 32$	20
2.1	Source locations and amplitudes	27
2.2	Evaluation of the potential with respect to P	29
2.3	the source locations with respect to reference point	30
2.4	Error Analysis for the Green's function	33
2.5	Error analysis for the potential	35
3.1	Evaluation of the potential at \vec{r}_Q where $ \vec{r}_Q < \vec{r}_{QK} $	38
3.2	Evaluation of the potential at \vec{r}_Q where $ \vec{r}_Q > \vec{r}_{QK} $	40
3.3	Vector representation for translation method	41
3.4	Error analysis for cube shape	43

3.5	Relative error versus truncation order for cubically shaped subdomains	46
3.6	Error analysis for sphere shape cluster	49
3.7	Translation error analysis for spherically shaped subdomains with dif- ferent buffer boxes	50

NOMENCLATURE

ϕ Azimuthal angle

θ Polar angle

\vec{k} Wavenumber vector

\vec{r} Position vector

a_{nm} Expansion coefficient

G Green's function in time domain

g Green's function in frequency domain

$H_n(r)$ Ordinary Hankel function, order n

$h_n^{(1)}(r)$ Spherical Hankel function of 1st kind, order n

$J_n(r)$ Ordinary Bessel function of 1st kind, order n

$j_n(r)$ Spherical Bessel function of 1st kind, order n

N Number of particles

P_n Legendre polynomial, order n

P_n^m Associated Legendre Polynomial

R_n^m Regular solution

S_n^m Singular solution

T Truncation order

w Frequency radian per second

x, y, z Cartesian coordinates

$y_n(r)$ Spherical Bessel function of 2^{nd} kind, order n

$Y_n(r)$ Ordinary Bessel function of 2^{nd} kind, order n

δ Delta function

O Operation count

$Y_{nm}(\theta, \phi)$ Spherical harmonics, order n , degree m

$Y_{nm}^*(\theta, \phi)$ Complex conjugate of spherical harmonics, order n , degree m

0.1 Background

There are numerous approaches that can be used to solve numerically the Helmholtz and wave equations [1–3]. For bounded problem domains, the finite element method(FEM) and the finite difference method(FDM) methods are used . In cases, where problem domain is unbounded integral equation methods are attractive, since the Sommerfeld radiation condition can be easily made to satisfy [4].

Integral equations such as the Kirchhoff integral is an exact solution to the Helmholtz equation for boundary problem. The discretization of the integral yields a system of linear equations and the integral solution is the result of a matrix-vector product. Rokhlin and Greengard [5] examined the fast multipole method(FMM) as a way to speed up the integral calculation. Consider the N -body problem where one wishes to calculate the potential at N points resulting from the contribution of N particles. The time-complexity of a naive algorithm is $O(N^2)$ [6], because all pairs of points need to be considered in N -body problem [7,8]. Using the FMM the computational complexity for the matrix-vector product reduces to the $O(N)$ [1,5]. FMM has applications in many fields.

In the paper entitled Fast Multipole Method Numerical Implementation by E. Darve [9], the FMM was used to perform the matrix-vector multiplication with $O(N)$ number of operations [10,11]. Rokhlin and Greengard [5,12] developed an algorithm for the rapid evaluation of the potential and the force field in the system which consists of a large number of particles. The CPU time for this algorithm was

$O(N)$ where N is the number of particles [13].

Use of the FMM to solve various types of partial differential equations is introduced in [1] by Yoshida. Rokhlin [14] presented an algorithm for the rapid solution of boundary value problems for the Helmholtz equation in two dimensions. The time complexity of the algorithm is $O(N^{4/3})$ where N is number of particles. FMM efficiently solved wave scattering problems and has been adapted to the solution of the integral equation for electromagnetic scattering problems in two dimensions [15]. The running time for solving the integral equation is $O(N^3)$ and by the FMM it can be reduced to $O(N^{4/3})$. The Laplace equation in three dimensions is also solved using the FMM [16].

When subdomains are used, the FMM loses the accuracy when subdomain centers are closer to one wavelength. This state of affair is caused by the behavior of the spherical Bessel function of the second kind when its order is greater than its argument [17].

0.2 Objective

The objective of the thesis is examine the cause of error in the FMM method. Of particular interest the approximation error in the Green's function and in the subdomain translation process is emphasized. The translation method is critical for efficient implementation of the FMM and is required when the computational domain is subdivided into subdomains [18]. Each subdomain the translation coefficients are calculated using the Gaunt function [19]. It can be an efficient method but the calculation can be prone to inaccuracy.

0.3 Organization of the Thesis

In Chapter 2, the solution to the Helmholtz equation in Cartesian and Spherical coordinate systems is derived. Error analysis between the free space and spherical Green's function is studied. In Chapter 3, the Fast Multipole Method is introduced and the Kirchhoff integral formula as a solution to the Helmholtz equation is derived. The expansion coefficients are introduced and the accuracy of the coefficients for the Green's function and the expression for potential is evaluated. In Chapter 4, the translation process is developed and translation error analyzed for the single level fast multipole method.

CHAPTER 1

SOLUTION TO THE HELMHOLTZ EQUATION

1.1 Introduction

The study of acoustics requires one to solve the Helmholtz equation in three dimensions [11]. Taking the Fourier transform of the wave equation in time yields the Helmholtz equation [20].

$$\nabla^2 \Phi + \gamma^2 \Phi = 0 \quad (1.1)$$

where Φ is the velocity potential, $\gamma = \omega/c$, γ is the wavenumber, ω is the angular frequency, c is the speed of sound and ∇^2 is the Laplace operator.

1.2 Solution of the Helmholtz Equation in Cartesian Coordinates

In this section, we will outline the process used to determine the solution of the inhomogeneous Helmholtz equation

$$\nabla^2 g + \gamma^2 g = -\delta(\vec{r} - \vec{r}_0) \quad (1.2)$$

where $g(\vec{r}, \vec{r}_0)$ is the Green's function. The observer and source locations are \vec{r} and \vec{r}_0 , respectively. The solution of Eqn (1.2) will be obtained implementing the three-dimensional spatial Fourier transform. The Fourier transform pair for the Green's

function will be denoted as $g(\vec{r}, \vec{r}_0) \leftrightarrow G(\vec{k}, \vec{r}_0)$. The inverse Fourier transform is given by

$$g(\vec{r}, \vec{r}_0) = \frac{1}{(2\pi)^3} \int_{-\infty}^{+\infty} \int_{-\infty}^{+\infty} \int_{-\infty}^{+\infty} G(\vec{k}, \vec{r}_0) e^{i\vec{k} \cdot \vec{r}} d\vec{k} \quad (1.3)$$

whereas the forward Fourier transform is defined as

$$G(\vec{k}, \vec{r}_0) = \int_{-\infty}^{+\infty} \int_{-\infty}^{+\infty} \int_{-\infty}^{+\infty} g(\vec{r}, \vec{r}_0) e^{-i\vec{k} \cdot \vec{r}} d\vec{r} \quad (1.4)$$

where spatial wavenumber vector $\vec{k} = (k_x, k_y, k_z)$.

Expressing each term in Eqn (1.2) in terms of its inverse spatial Fourier transform yields

$$\delta(\vec{r} - \vec{r}_0) = \frac{1}{(2\pi)^3} \int_{-\infty}^{+\infty} \int_{-\infty}^{+\infty} \int_{-\infty}^{+\infty} e^{i\vec{k} \cdot (\vec{r} - \vec{r}_0)} d\vec{k} \quad (1.5)$$

$$\nabla^2 g = - \frac{1}{(2\pi)^3} \int_{-\infty}^{+\infty} \int_{-\infty}^{+\infty} \int_{-\infty}^{+\infty} G(\vec{k}, \vec{r}_0) e^{i\vec{k} \cdot \vec{r}} d\vec{k} \quad (1.6)$$

Substituting Eqns (1.3,1.5,1.6) into Eqn (1.2) yields

$$\frac{1}{(2\pi)^3} \int_{-\infty}^{+\infty} \int_{-\infty}^{+\infty} \int_{-\infty}^{+\infty} \left[(\gamma^2 - k^2) G - e^{-i\vec{k} \cdot \vec{r}_0} \right] e^{i\vec{k} \cdot \vec{r}} d\vec{k} = 0 \quad (1.7)$$

As we can see, Eqn (1.7) is equal to zero for all choices for the source and observation points. In other words, the integral is invariant to changes to the spatial variables.

The only way this can occur is if the integrand itself is equal to zero. Hence

$$G = \frac{e^{-i\vec{k} \cdot \vec{r}_0}}{(k^2 - \gamma^2)} \quad (1.8)$$

where $k = |\vec{k}|$. The task at hand is to obtain g . This will be done by taking the inverse Fourier transform of G . The application of complex variable analysis will aid us in this task. The Green's function is equal to

$$g = \frac{1}{(2\pi)^3} \int_{-\infty}^{+\infty} \int_{-\infty}^{+\infty} \left[\int_{-\infty}^{+\infty} \left(\frac{e^{ik_z(z-z_0)}}{k^2 - \gamma^2} \right) dk_z \right] e^{ik_x(x-x_0)} e^{ik_y(y-y_0)} dk_y dk_x \quad (1.9)$$

The integral in the square brackets in Eqn (1.9) will be examined first. We will use the term the integral I_z for reference.

$$I_z = \frac{1}{(2\pi)^3} \int_{-\infty}^{+\infty} \frac{e^{ik_z(z-z_0)}}{k_z^2 + k_x^2 + k_y^2 - \gamma^2} dk_z \quad (1.10)$$

The integrand has two poles on the imaginary axis in the complex k_z plane namely

$$k_z = \pm i \sqrt{k_x^2 + k_y^2 - \gamma^2} \quad (1.11)$$

Recognizing that the integrand of Eqn (1.10) decays as $1/|k_z|^2$ in the limit as $|k_z|$ approaches infinity, the integral along the real line may be evaluated using a suitably chosen contour integral. In Fig (1.1), the poles are plotted and the contour used for each spatial region of $z - z_0$ is shown.

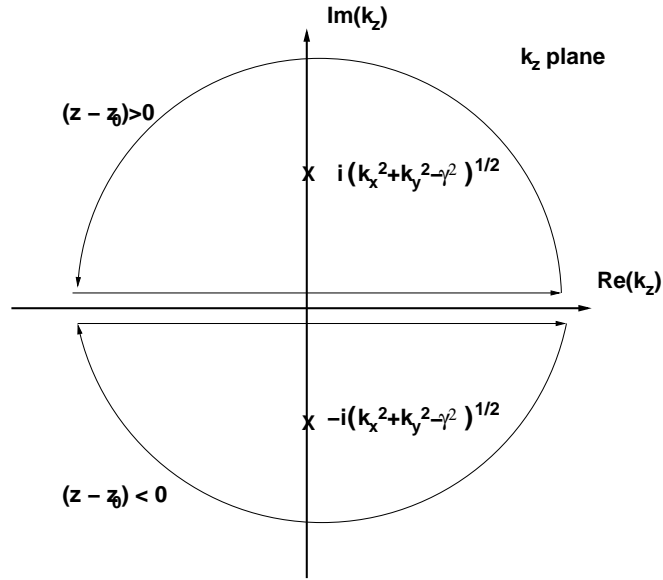


Figure 1.1: Contour integral

To ensure convergence of the integral, based on the sign of $(z - z_0)$, one must

close the contour in either the upper or lower half-plane.

$$I_z = \begin{cases} \frac{1}{8\pi^2} \frac{e^{-\sqrt{k_x^2 + k_y^2 - \gamma^2}(z-z_0)}}{\sqrt{k_x^2 + k_y^2 - \gamma^2}} & \text{if } z - z_0 > 0 \\ \frac{1}{8\pi^2} \frac{e^{\sqrt{k_x^2 + k_y^2 - \gamma^2}(z-z_0)}}{\sqrt{k_x^2 + k_y^2 - \gamma^2}} & \text{if } z - z_0 < 0 \end{cases} \quad (1.12)$$

Hence the I_z given in Eqn(1.10) is equal to

$$I_z = \frac{1}{8\pi^2} \frac{e^{-\sqrt{k_x^2 + k_y^2 - \gamma^2} |z-z_0|}}{\sqrt{k_x^2 + k_y^2 - \gamma^2}} \quad (1.13)$$

Now we will integrate Eqn (1.9) with respect to k_x and k_y coordinates. Eqn (1.9) can be rewritten as follows,

$$g = \frac{1}{8\pi^2} \int_{-\infty}^{+\infty} \int_{-\infty}^{+\infty} \frac{e^{ik_x X} e^{ik_y Y} e^{-\sqrt{k_x^2 + k_y^2 - \gamma^2} |z-z_0|}}{\sqrt{k_x^2 + k_y^2 - \gamma^2}} dk_x dk_y \quad (1.14)$$

where $X = x - x_0$ and $Y = y - y_0$. It is advantageous to use a cylindrical coordinate representation of the two-dimensional wavenumber integration. Converting Eqn (1.14) to a cylindrical coordinate system yields

$$g = \frac{1}{8\pi^2} \int_0^{+\infty} \int_0^{+\infty} \frac{e^{iK\rho[\cos(\beta)\cos(\theta)+\sin(\beta)\sin(\theta)]} e^{-\sqrt{K^2\cos^2(\beta)+K^2\sin^2(\beta)-\gamma^2} |z-z_0|}}{\sqrt{K^2\cos^2(\beta)+K^2\sin^2(\beta)-\gamma^2}} K dK d\beta \quad (1.15)$$

where

$$\begin{aligned} X &= \rho \cos(\theta), \quad Y = \rho \sin(\theta) \\ k_x &= K \cos(\beta), \quad k_y = K \sin(\beta) \\ K &= \sqrt{k_x^2 + k_y^2}, \quad \rho = \sqrt{X^2 + Y^2} \end{aligned} \quad (1.16)$$

$$g = \frac{1}{8\pi^2} \int_0^{+\infty} \int_0^{2\pi} \frac{e^{iK\rho[\cos(\beta)\cos(\theta)+\sin(\beta)\sin(\theta)]} e^{-\sqrt{K^2-\gamma^2} |z-z_0|}}{\sqrt{K^2-\gamma^2}} K dK d\beta \quad (1.17)$$

$$g = \frac{1}{8\pi^2} \int_0^{+\infty} \left[\int_0^{2\pi} e^{iK\rho \cos(\beta-\theta)} d\beta \right] \frac{e^{-\sqrt{K^2-\gamma^2} |z-z_0|}}{\sqrt{K^2-\gamma^2}} K dK \quad (1.18)$$

The bracketed integral in Eqn (1.18) can be expressed in terms of the zeroth order Bessel function of the first kind J_0 .

$$\int_0^{2\pi} e^{iK\rho \cos(\beta-\theta)} d\beta = 2\pi J_0(K\rho) \quad (1.19)$$

Substituting Eqn (1.19) into Eqn (1.18) yields the Hankel transform

$$g = \frac{1}{4\pi} \int_0^{+\infty} \frac{e^{-\sqrt{K^2-\gamma^2} |z-z_0|}}{\sqrt{K^2-\gamma^2}} J_0(K\rho) K dK \quad (1.20)$$

We will split the integral into two parts such that

$$g = \frac{1}{4\pi} [g_1 + g_2] \quad (1.21)$$

where the terms of the aforementioned equation are

$$g_1 = \int_0^\gamma i \frac{e^{i\sqrt{\gamma^2-K^2} |z-z_0|}}{\sqrt{\gamma^2-K^2}} J_0(K\rho) K dK \quad (1.22)$$

$$g_2 = \int_\gamma^\infty \frac{e^{-\sqrt{K^2-\gamma^2} |z-z_0|}}{\sqrt{K^2-\gamma^2}} J_0(K\rho) K dK \quad (1.23)$$

Using Euler's identity and the change of variables $a = K/\gamma$, $da = \frac{dK}{\gamma}$, $b = \gamma|z-z_0|$

and $c = \gamma\rho$

$$g_1 = \int_0^1 \frac{i\gamma \cos(b\sqrt{1-a^2})}{\sqrt{1-a^2}} J_0(ac) a da - \int_0^1 \frac{\gamma \sin(b\sqrt{1-a^2})}{\sqrt{1-a^2}} J_0(ac) a da \quad (1.24)$$

$$g_2 = \int_1^\infty \frac{\gamma e^{-b\sqrt{a^2-1}}}{\sqrt{a^2-1}} J_0(ac) a da \quad (1.25)$$

We will evaluate the imaginary part and real part of $g_1 + g_2$ separately. The imaginary part of the sum is evaluated in [21, p. 40(48)] and simplified using auxiliary properties in [22]. The result may be written as

$$Im(g_1 + g_2) = \int_0^1 \frac{\gamma \cos(b\sqrt{1-a^2})}{\sqrt{1-a^2}} J_0(ac) a \, da = \frac{\gamma \sin(\sqrt{b^2+c^2})}{\sqrt{b^2+c^2}} \quad (1.26)$$

The real part of $g_1 + g_2$ can be evaluated using [21, p. 35(23)] and simplified using the spherical Bessel function relations given in [22, p. 438(10.1.11), p. 438(10.1.12)].

The result is equal to

$$\begin{aligned} Re(g_1 + g_2) &= - \int_0^1 \frac{\gamma \sin(b\sqrt{1-a^2})}{\sqrt{1-a^2}} J_0(ac) a \, da + \int_1^\infty \frac{\gamma e^{-b\sqrt{a^2-1}}}{\sqrt{a^2-1}} J_0(ac) a \, da \\ &= \frac{\gamma \cos(\sqrt{b^2+c^2})}{\sqrt{b^2+c^2}} \end{aligned} \quad (1.27)$$

Finally, the Green's function can be evaluated by adding the real and imaginary parts of the Green's function and dividing by 4π .

$$g = \frac{\gamma e^{i\sqrt{b^2+c^2}}}{4\pi\sqrt{b^2+c^2}} = \frac{e^{i\gamma R}}{4\pi R} \quad (1.28)$$

where $R = |\vec{r} - \vec{r}_0|$ is the distance between source and observation positions.

1.3 Green's Function for the Helmholtz Equation in terms of Spherical Harmonics

The Helmholtz equation in spherical coordinates [23–25] is

$$\begin{aligned} \frac{1}{r^2} \frac{\partial}{\partial r} \left(r^2 \frac{\partial g}{\partial r} \right) + \frac{1}{r^2 \sin(\theta)} \frac{\partial}{\partial \theta} \left(\sin(\theta) \frac{\partial g}{\partial \theta} \right) + \frac{1}{r^2 \sin^2(\theta)} \frac{\partial^2 g}{\partial \phi^2} + \gamma^2 g \\ = -\frac{\delta(r - r_o)}{r^2} \delta(\phi - \phi_o) \delta(\theta - \theta_o) \end{aligned} \quad (1.29)$$

In the above equation, (r, θ, ϕ) and (r_o, θ_o, ϕ_o) are the spherical coordinates of the observation point and the source point, respectively. The range of variables are $(0 \leq \phi \leq 2\pi)$, $(0 \leq \theta \leq \pi)$ and $r \geq 0$.

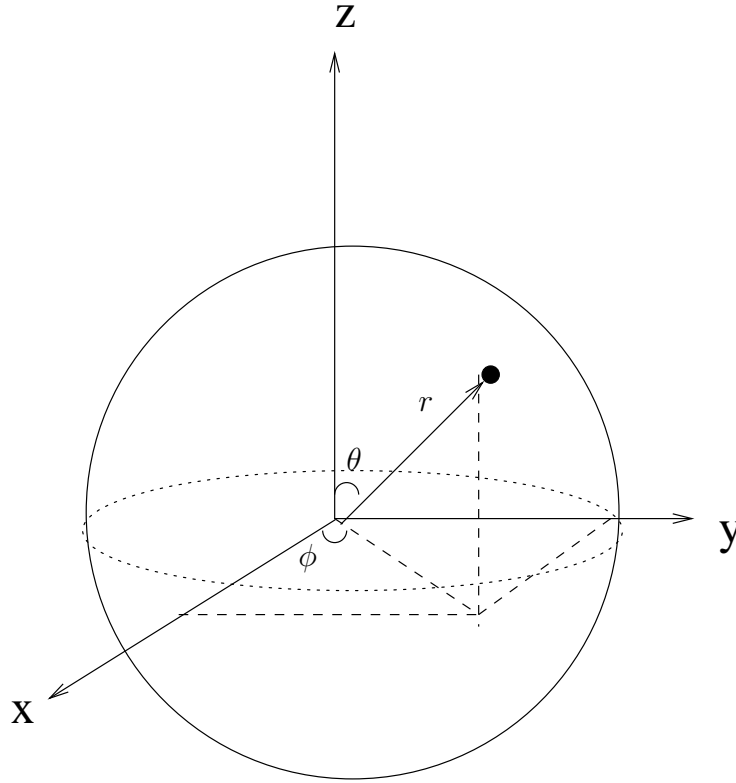


Figure 1.2: Spherical coordinate system

In order to find the expression for the Green's function, we need to derive the solution to the inhomogeneous Helmholtz equation. The inhomogeneous solution can

be obtained using the separation of variables method, where

$$g(r, \theta, \phi) = R(r)\Theta(\theta)\Phi(\phi). \quad (1.30)$$

$R(r)$ is a solution with variable r , $\Theta(\theta)$ is a solution with variable θ and $\Phi(\phi)$ is a solution with variable ϕ . Appendix 1 shows derivation of the solution by representing g as,

$$g = \sum_{n=0}^{\infty} \sum_{m=-n}^n a_{nm} R_n(r) Y_{nm}(\theta, \phi) \quad (1.31)$$

where a_{nm} are the coefficients of the expansion. The function $Y_{nm}(\theta, \phi)$ is the spherical harmonic given by $Y_{nm}(\theta, \phi) = P_{nm}(\cos(\theta))e^{im\phi}/\sqrt{2\pi}$, where P_{nm} is the normalized associated Legendre polynomial of order n and degree m . Our aim is to find the unknown coefficient a_{nm} and the expression for $R_n(r)$ which is a function of radial distance r . Substituting Eqn(1.30) in place of g in Eqn (1.29) yields.

$$\sum_{n=0}^{\infty} \sum_{m=-n}^n a_{nm} \frac{1}{r^2} [(r^2 R'_n)' + (\gamma^2 r^2 - n(n+1))R_n] Y_{nm} = \frac{\delta(r - r_o)}{r^2} \delta(\phi - \phi_o) \delta(\theta - \theta_o) \quad (1.32)$$

where $()'$ denote differentiation with respect to the argument. In order to determine a_{nm} , we multiply both sides of the equation by $\sin(\theta)d\theta d\phi Y_{qj}^*$ where Y_{qj}^* is complex conjugate of Y_{qj} . Integrating the result over $\phi : (0, 2\pi)$ and $\theta : (0, \pi)$ yields by virtue of orthogonality of Y_{nm}

$$\int_0^{2\pi} \int_0^{\pi} Y_{nm}(\theta, \phi) Y_{qj}^*(\theta, \phi) \sin(\theta) d\theta d\phi = \begin{cases} 1, & \text{if } n=m, q=j \\ 0, & \text{otherwise} \end{cases} \quad (1.33)$$

In the above equation, substituting $\zeta = \cos(\theta)$ and $d\zeta = -\sin(\theta)d\theta$ yields

$$\int_0^{2\pi} \int_{-1}^1 Y_{nm}(\zeta, \phi) Y_{qj}^*(\zeta, \phi) d\zeta d\phi = \begin{cases} 1, & \text{if } n=m, q=j \\ 0, & \text{otherwise} \end{cases} \quad (1.34)$$

Therefore Eqn(1.32) becomes

$$a_{nm} [R_n'' + 2R_n'/r + (\gamma^2 - n(n+1)/r^2)R_n] = -\frac{\delta(r - r_o)}{r^2} Y_{nm}^*(\zeta_o, \phi_o) \quad (1.35)$$

In the above equation, equating the radial terms yields coefficient a_{nm} equal to the complex conjugate of the spherical harmonic Y_{nm}^* as follows:

$$a_{nm} = Y_{nm}^*(\zeta_o, \phi_o) \quad (1.36)$$

Derivation of the expansion coefficients for the radial solutions to the Helmholtz equation is as follows. Isolating the radial terms in Eqn (1.32) yields the following Bessel differential equation.

$$[R_n'' + 2R_n'/r + (\gamma^2 - n(n+1)/r^2)R_n] = -\frac{\delta(r - r_o)}{r^2} \quad (1.37)$$

Solutions to the Bessel equation are the spherical Bessel functions of first kind $j_n(\gamma r)$ and second kind $y_n(\gamma r)$ [26]. There are two solutions of Eqn (1.37), i.e. $R_n(r)$ depending on the distance of r with relative to r_0 .

For $r < r_0$

$$R_n(r) = B j_n(\gamma r) \quad (1.38)$$

for $r > r_0$

$$R_n(r) = A h_n^{(1)}(\gamma r) \quad (1.39)$$

where A and B are constants. Also $h_n^{(1)}(\gamma r)$ is the spherical Hankel function of the first kind [26, 27] and given by $h_n^{(1)}(\gamma r) = j_n(\gamma r) + iy_n(\gamma r)$. Considering Eqns (1.38 and 1.39), the condition for the continuity of the radial solution can be written as

$$A h_n^{(1)}(\gamma r_0) - B j_n(\gamma r_0) = 0 \quad (1.40)$$

At $r = r_0$, R'_n is discontinuous, so at this point we will use a jump condition which can be derived as follows. Integrating Eqn (1.37) over $r = (r_0 - \epsilon, r_0 + \epsilon)$ and using the impulse-matching technique yields

$$\lim_{\epsilon \rightarrow 0} R'_n(r) \Big|_{(r_0 - \epsilon)}^{(r_0 + \epsilon)} = \frac{-1}{r_0^2} \quad (1.41)$$

Hence the radial solution $R'_n(r)$ satisfies

$$A \gamma h_n'^{(1)}(\gamma r_0) - B \gamma j_n'(\gamma r_0) = \frac{-1}{r_0^2} \quad (1.42)$$

From Eqns (1.40 and 1.42) we have two equations which can be written in matrix form as

$$\begin{bmatrix} -h_n^{(1)}(\gamma r_0) & j_n(\gamma r_0) \\ -h_n'^{(1)}(\gamma r_0) & j_n'(\gamma r_0) \end{bmatrix} \begin{bmatrix} A \\ B \end{bmatrix} = \begin{bmatrix} 0 \\ \frac{1}{\gamma r_0^2} \end{bmatrix} \quad (1.43)$$

$$A = \frac{-j_n(\gamma r_0)}{-h_n^{(1)}(\gamma r_0)j_n'(\gamma r_0) + h_n'^{(1)}(\gamma r_0)j_n(\gamma r_0)} \frac{1}{\gamma r_0^2} \quad (1.44)$$

$$B = \frac{-h_n^{(1)}(\gamma r_0)}{-h_n^{(1)}(\gamma r_0)j_n'(\gamma r_0) + h_n'^{(1)}(\gamma r_0)j_n(\gamma r_0)} \frac{1}{\gamma r_0^2} \quad (1.45)$$

Where $()'$ denote differentiation with respect to the argument. The above matrix can be simplified using the Wronskian determinant [28], yielding

$$-h_n^{(1)}(\gamma r_0)j_n'(\gamma r_0) + h_n'^{(1)}(\gamma r_0)j_n(\gamma r_0) = \frac{-i}{\gamma^2 r_0^2} \quad (1.46)$$

Substituting the above determinant in Eqns (1.44 and 1.45) gives

$$A = j_n(\gamma r_0)(+i\gamma) \quad (1.47)$$

$$B = h_n^{(1)}(\gamma r_0)(+i\gamma) \quad (1.48)$$

Substituting the solution for A and B into Eqns (1.38 and 1.39) the radial solution is obtained.

For $r > r_0$

$$R_n(r) = (+i\gamma)j_n(\gamma r_0)h_n^{(1)}(\gamma r) \quad (1.49)$$

and for $r < r_0$

$$R_n(r) = (+i\gamma)h_n^{(1)}(\gamma r_0)j_n(\gamma r) \quad (1.50)$$

Combining the solutions of the Helmholtz equation in Eqn (1.31) with Eqns (1.49 and 1.50) yields the following expression for the spherical Green's function.

$$g = \begin{cases} i\gamma \sum_{n=0}^{\infty} \sum_{m=-n}^n j_n(\gamma r_0)h_n^{(1)}(\gamma r)Y_{nm}(\zeta, \phi)Y_{nm}^*(\zeta_0, \phi_0) & \text{if } r > r_0 \\ i\gamma \sum_{n=0}^{\infty} \sum_{m=-n}^n j_n(\gamma r)h_n^{(1)}(\gamma r_0)Y_{nm}(\zeta, \phi)Y_{nm}^*(\zeta_0, \phi_0) & \text{if } r_0 > r \end{cases} \quad (1.51)$$

Eqn (1.51) can be rewritten using following expressions.

$$R_n^m(\vec{r}) = j_n(\gamma r)Y_{nm}(\zeta, \phi) \quad (1.52)$$

$$S_n^m(\vec{r}) = h_n^{(1)}(\gamma r)Y_{nm}(\zeta, \phi) \quad (1.53)$$

Noting the $Y_{nm}^* = Y_{n,-m}$, the spherical Green's function is given by

$$g = \begin{cases} i\gamma \sum_{n=0}^{\infty} \sum_{m=-n}^n S_n^m(\vec{r})R_n^{-m}(\vec{r}_0) & \text{if } |\vec{r}| > |\vec{r}_0| \\ i\gamma \sum_{n=0}^{\infty} \sum_{m=-n}^n S_n^{-m}(\vec{r}_0)R_n^m(\vec{r}) & \text{if } |\vec{r}| < |\vec{r}_0| \end{cases} \quad (1.54)$$

For the numerical computation the series is truncated. Therefore Eqn (1.54) can be rewritten as

$$g = \begin{cases} i\gamma \sum_{n=0}^T \sum_{m=-n}^n S_n^m(\vec{r}) R_n^{-m}(\vec{r}_0) & \text{if } |\vec{r}| > |\vec{r}_0| \\ i\gamma \sum_{n=0}^T \sum_{m=-n}^n S_n^{-m}(\vec{r}_0) R_n^m(\vec{r}) & \text{if } |\vec{r}| < |\vec{r}_0| \end{cases} \quad (1.55)$$

Where \vec{r} and \vec{r}_0 are the position vectors of the observation and source points respectively, where T is the truncation order. Also, n is the order and m is the degree.

S is the singular basis function and R is the regular basis function which represents solution to the Helmholtz equation. Regular solution $R_n^m(\vec{r})$ is regular everywhere and singular solution $S_n^m(\vec{r})$ is singular when $r = 0$ due to the Hankel function. Singular and regular solutions separate the domain of solutions as shown in Figs (1.3 and 1.4). For the sphere of radius a , R is the regular solution inside the sphere and S is the singular solution outside the sphere. The spherical Green's function formula for the case when $|\vec{r}| > |\vec{r}_0|$ is referred as far field or multipole expansion as shown in Fig (1.3). For the case when $|\vec{r}| < |\vec{r}_0|$ is referred as near field or local expansion as shown in Fig (1.4).

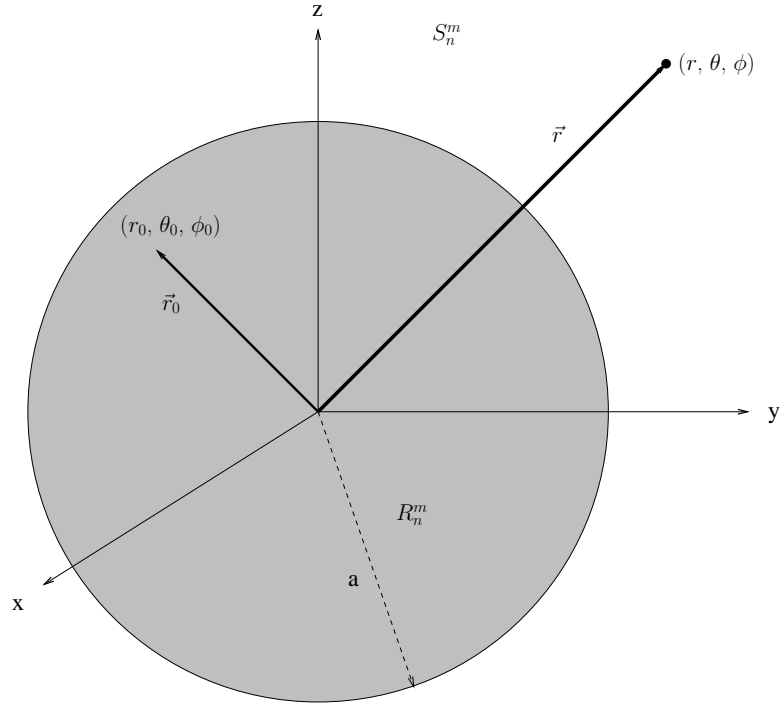


Figure 1.3: Regular and singular solutions for $|\vec{r}| > |\vec{r}_0|$

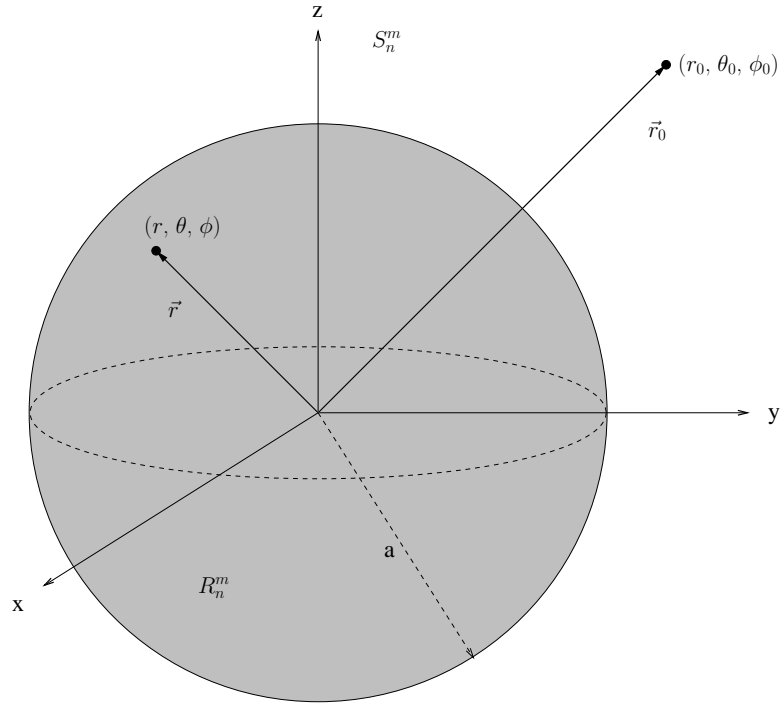


Figure 1.4: Regular and singular solutions for $|\vec{r}| < |\vec{r}_0|$

1.4 Approximation Error

In this section, we will examine the error due to the approximation of the free space Green's function in spherical coordinates. Using Eqns (1.28 and 1.55) the approximation for the free space Green's function in spherical coordinates is given as

$$g(\vec{r}, \vec{r}_0) = \frac{e^{ik|\vec{r}-\vec{r}_0|}}{4\pi|\vec{r}-\vec{r}_0|} \simeq \begin{cases} i\gamma \sum_{n=0}^T \sum_{m=-n}^n S_n^m(\vec{r}) R_n^{-m}(\vec{r}_0) & \text{if } |\vec{r}| > |\vec{r}_0| \\ i\gamma \sum_{n=0}^T \sum_{m=-n}^n S_n^{-m}(\vec{r}_0) R_n^m(\vec{r}) & \text{if } |\vec{r}| < |\vec{r}_0| \end{cases} \quad (1.56)$$

where \vec{r} and \vec{r}_0 are the locations for the observation point and source point respectively. The approximation of the free space Green's function in spherical coordinates is the series of the regular and singular functions. This series is truncated for numerical computation. In Eqn (1.56), the series is truncated at T which is referred to as the truncation number. From the series, we can see that the truncation number is directly proportional to the convergence of the series. Therefore, if the truncation number is large, the series converges and the error between the free space Green's function and spherical Green's function decreases. By using Eqn (1.56), the approximation error analysis of the Green's function with respect to the truncation number is considered.

Use of Eqn (1.56) for the approximation error analysis results in a singularity due to the $|\vec{r}-\vec{r}_0|$ term in the denominator of the expression for the free space Green's function. To examine the error irrespective of the singularity, a different expression is considered for the free space and spherical Green's function where the $|\vec{r}-\vec{r}_0|$ term

does not give rise to a singularity. The aforementioned expression is given as

$$g_f(\vec{r}, \vec{r}_0) = |\vec{r} - \vec{r}_0| \quad g(\vec{r}, \vec{r}_0) = \frac{e^{ik|\vec{r}-\vec{r}_0|}}{4\pi} \quad (1.57)$$

$$g_s(\vec{r}, \vec{r}_0) \simeq \begin{cases} i\gamma |\vec{r} - \vec{r}_0| \sum_{n=0}^T \sum_{m=-n}^n S_n^m(\vec{r}) R_n^{-m}(\vec{r}_0) & \text{if } |\vec{r}| > |\vec{r}_0| \\ i\gamma |\vec{r} - \vec{r}_0| \sum_{n=0}^T \sum_{m=-n}^n S_n^{-m}(\vec{r}_0) R_n^m(\vec{r}) & \text{if } |\vec{r}| < |\vec{r}_0| \end{cases} \quad (1.58)$$

where $g_f(\vec{r}, \vec{r}_0)$ and $g_s(\vec{r}, \vec{r}_0)$ represents free space and spherical Green's function respectively. In Eqn (1.57), $|\vec{r} - \vec{r}_0|$ is removed from the denominator therefore the absolute value of the free space Green's function $g_f(\vec{r}, \vec{r}_0)$ is constant with a value of $\frac{1}{4\pi}$. In order to approximate the free space Green's function in spherical coordinates, the expression for the spherical Green's function $g(\vec{r}, \vec{r}_0)$ is multiplied with $|\vec{r} - \vec{r}_0|$ in Eqn (1.58). The relative error between the free and spherical Green's function is calculated using $\frac{g_f - g_s}{g_f}$. As spherical Green's function is a series, it does not converge for all points located at a distance equal to the radius \vec{r}_0 . Therefore, in Figs (1.5 and 1.6) we see that for the locations equal to \vec{r}_0 , the series does not converge and error is maximum.

For the analysis of the approximation error, the following experiment is performed. A 2D grid is considered ranging from -20 to 20 for the x-axis and y-axis. The total number of points is 80. Relative error is plotted on the z axis. All the grid points are observation points except the source point which is located at $\vec{r}_0 = (10.1, 0, 0)$.

The relative error is calculated using Eqns (1.57 and 1.58). Figs (1.5 and 1.6) are the relative error plots for the truncation number $T = 16$ and $T = 32$ respectively. The results are plotted in Figs (1.5 and 1.6) with different truncation number in order

to clearly understand the decrease in the approximation error with the increase in truncation number.

Fig (1.5) shows that the maximum error occurs at the circle of radius equal to $\vec{r}_0 = (10.1, 0, 0)$ as the function does not converge at the circle. The error is minimum elsewhere. Also, the maximum relative error is 1.2.

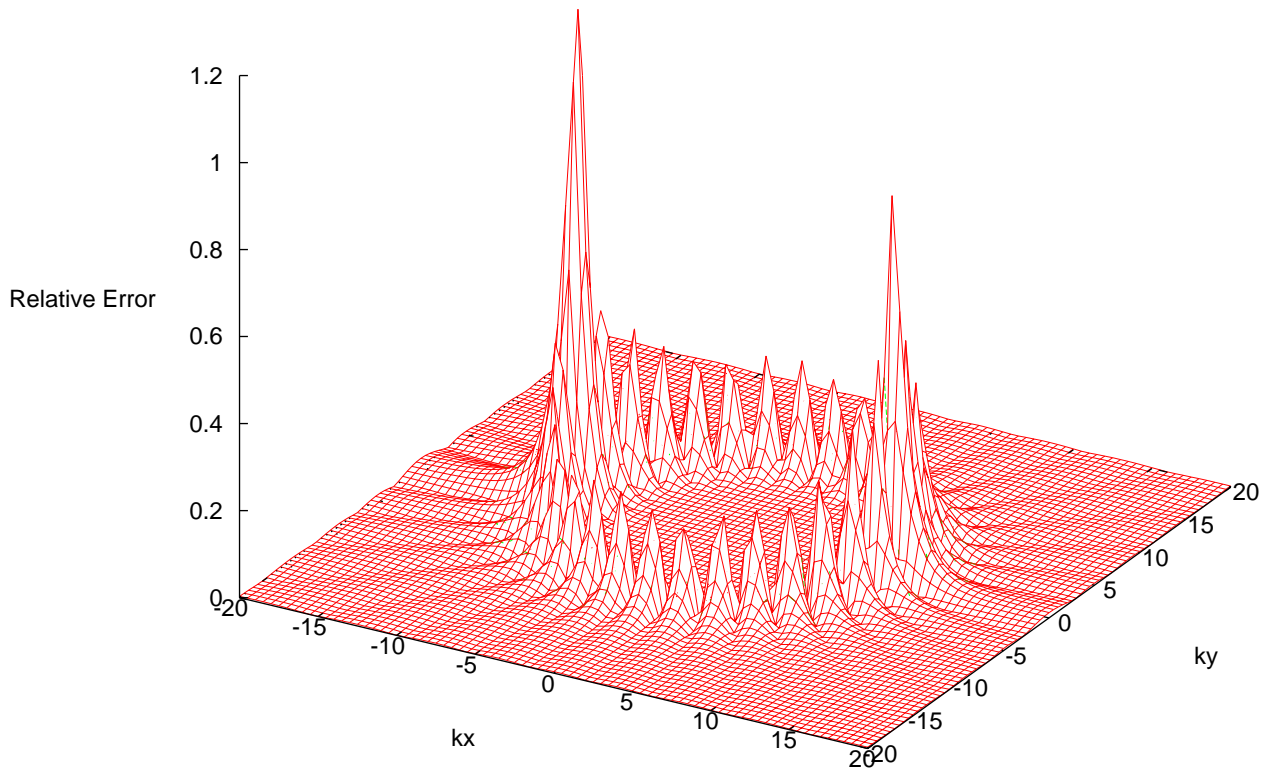


Figure 1.5: Approximation error for $T = 16$

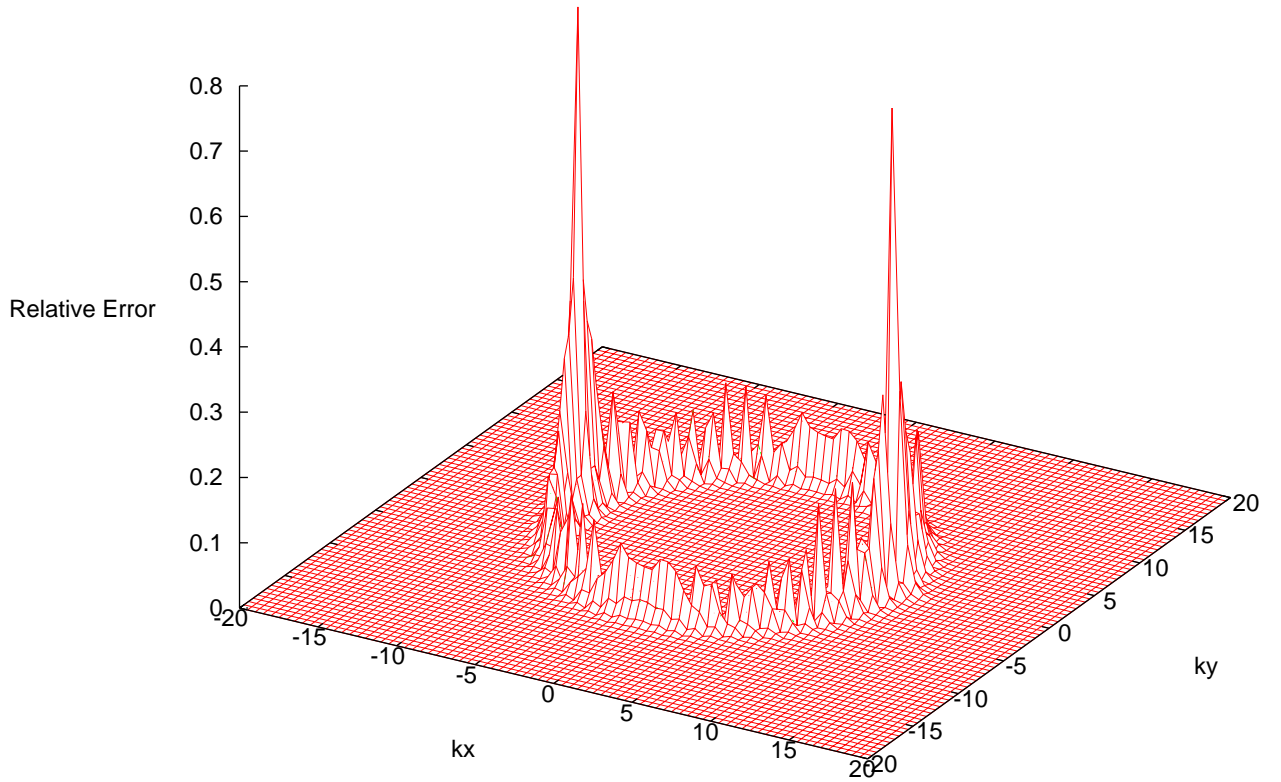


Figure 1.6: Approximation error for $T = 32$

Fig(1.6) shows that increasing the truncation number decreases the maximum relative error from 1.2 to 0.8. Therefore, the spherical Green's function is a good approximation for the free space Green's function.

1.5 Kirchhoff Integral Formula

In this section, the integral form of the solution of the inhomogeneous Helmholtz equation is derived [29] [30]. The Kirchhoff integral formula expresses the potential p in a closed volume V as the sum of contributions arising from the sources on the surface A of the volume V and those enclosed in the volume. The Kirchhoff integral formula [30] in the frequency domain is

$$p(\vec{r}_0, k) = \oint_A [g(\nabla p) \cdot \vec{n} - p(\nabla g) \cdot \vec{n}] dA + \int_V g s dV \quad (1.59)$$

where g is the Green's function, $k = \omega/c$, \vec{n} is the inward directed normal vector and s is the source. The variable A represents the area of the surface of the volume V . The Kirchhoff integral formula can be derived as follows. Consider the inhomogeneous Helmholtz equation in the volume V .

$$\nabla^2 p + \gamma^2 p = s(\vec{r}, \omega) \quad (1.60)$$

where p is the potential, s is the amplitude of the source and γ is the wavenumber.

The Green's function satisfies

$$\nabla^2 g + \gamma^2 g = -\delta(\vec{r} - \vec{r}_0) \quad (1.61)$$

where \vec{r} and \vec{r}_0 are the locations of the observation point and source point, respectively. Multiplying Eqn (1.60) with g and Eqn (1.61) with p and then subtracting the result yields

$$g \nabla^2 p - p \nabla^2 g - g s = p \delta(\vec{r} - \vec{r}_0) \quad (1.62)$$

Integrating Eqn. (1.62) over the volume V yields

$$-\int_V (g \nabla^2 p + p \nabla^2 g) dV - \int_V g s dV = \int_V p \delta(\vec{r} - \vec{r}_0) dV \quad (1.63)$$

Using the sifting property of the delta function [4], Eqn (1.63) can be rewritten as

$$-\int_V (g \nabla^2 p - p \nabla^2 g) dV + \int_V g s dV = \begin{cases} p(\vec{r}_0) & \text{if } \vec{r}_0 \text{ is in } V \\ 0 & \text{otherwise} \end{cases} \quad (1.64)$$

The first term on the left-hand side of Eqn (1.64), which is a volume integral, can be converted into a surface integral using Green's theorem. Green's theorem gives the relationship between the closed surface integral and the volume integral of the total volume enclosed by the surface.

$$\int_V (g \nabla^2 p - p \nabla^2 g) dV = \oint_A [g(\nabla p) \cdot \vec{n} - p(\nabla g) \cdot \vec{n}] dA \quad (1.65)$$

Substituting the above relationship into Eqn (1.64) yields

$$p(\vec{r}_0) = \oint_A [g(\nabla p) \cdot \vec{n} - p(\nabla g) \cdot \vec{n}] dA - \int_V g s dV \quad (1.66)$$

Eqn (1.66) is the Kirchhoff's integral formula which gives the unknown potential at the observation point. If conservation of linear momentum is applied $g(\nabla p) \cdot \vec{n}$ is equal to $i\omega\rho g\vec{u} \cdot \vec{n}$.

In the thesis we will focus on the evaluation of $p(\vec{r}_0) = \int_V g s dV$. In our case the integral takes the form $p(\vec{r}) = \int_V g(\vec{r}, \vec{r}_0) s(\vec{r}_0) dV$, where $p(\vec{r})$ is the potential at the observation point. For the numerical computation the integral is transformed to a discrete summation form which is explained in the Chapter3. Fast multipole method is used to calculate the discrete summation form of the potential as explained in the Chapter3.

CHAPTER 2

ERROR ANALYSIS FOR THE GREEN'S FUNCTION AND THE EXPANSION COEFFICIENT

2.1 Introduction

In this chapter, we will develop the Single Layer Fast Multipole Method (SLFMM) and its application to the solution of the Helmholtz equation. In this context, the Fast Multipole Method (FMM) has found application in the numerical analysis of problems arising in the fields of electromagnetics, acoustics, astronomy, molecular dynamics and fluid mechanics [31–33].

The FMM is used to evaluate an unknown potential function at a given spatial location that results from the interaction of a large number of source particles [34]. The Green's function $g(\vec{r}, \vec{r}_0)$ is used to evaluate the influence of each source at \vec{r}_0 on the observed potential at \vec{r} . Given N source particles and N_o observation points, a direct calculation of the potential at all the prescribed observation points can be evaluated as the matrix-vector multiplication.

$$p(\vec{r}) = \sum_{j=1}^N g(\vec{r}, \vec{r}_0) s_j$$

In such a case, the evaluation will require $O(N_o N)$ complex multiplications.

2.2 Multipole expansion

The multipole expansion relies heavily on the separability of the kernel function $g(x, y)$. In Chapter 2 separable expressions for the Green's function have been given for the three-dimensional Helmholtz equation case. The technical elements required for exploiting the aforementioned result will be given here using one-dimensional model. Consider the integral

$$p(x) = \int_a^b g(x, y) s(y) dy \quad (2.1)$$

where $s(y)$ is the source distribution function. The Green's function $g(x, y)$ depends on two variables the observation point x and the source point y . The objective is to evaluate $p(x)$. Let the observation point x_i is drawn from the set $x = \{x_1, x_2, \dots, x_{N_o}\}$ and the source point is drawn for $y = \{y_1, y_2, \dots, y_N\}$, then

$$p(x_i) = \sum_{j=1}^N g(x_i, y_j) s(y_j) w(y_j) \quad (2.2)$$

for $i = \{1, \dots, N_o\}$ and $w(y_j)$ is the quadrature weight at y_j . Solving for $p(x_i)$ using kernel $g(x, y)$ leads to $O(N^2)$ operations. In such case one will obtain p using $N_o N$ multiplications and $N_o(N - 1)$ additions.

To reduce the number of operations, the strategy is to represent $g(x, y)$ as a product of a function in x and a function in y .

$$g(x, y) = \sum_{l=0}^M f_l(x) q_l(y) \quad (2.3)$$

where $f_l(x)$ and $q_l(y)$ are functions depending on x and y respectively. Calculating the integral requires discretization of the integrand. Discretizing the function $s(y)$

as follows.

$$s(y) = \sum_{j=1}^N \delta(y - y_j) s(y) w(y) \quad (2.4)$$

Substituting Eqn (2.4) into Eqn (2.1) yields

$$\begin{aligned} p(x) &= \int_a^b g(x, y) \sum_{j=1}^N \delta(y - y_j) s(y) w(y) dy \\ &= \sum_{j=1}^N g(x, y_j) s(y_j) w(y_j) \end{aligned} \quad (2.5)$$

kernel $g(x, y_j)$ as

$$g(x, y_j) = \sum_{l=0}^M f_l(x) q_l(y_j) \quad (2.6)$$

Substituting Eqn (2.6) into Eqn (2.5) yields

$$p(x) = \sum_{j=1}^N \sum_{l=0}^M f_l(x) q_l(y_j) w(y_j) s(y_j) \quad (2.7)$$

Grouping the terms which are dependent on y_j only

$$a_l = \sum_{j=1}^N q_l(y_j) w(y_j) s(y_j) \quad (2.8)$$

Substituting a_l in Eqn (2.7) gives

$$p(x) = \sum_{l=0}^M a_l f_l(x) \quad (2.9)$$

where a_l is a constant. The number of operations required to calculate each a_l is $O(N)$ and to calculate $p(x)$ are $O(M + 1)$. The coefficients a_l only needs to be calculated once which is a non-recurring cost of NM multiplications. Once the coefficients are evaluated each $p(x_i)$ requires $(M + 1)$ multiplications and M additions. As a result, p is evaluated at a cost of $O(N_o(M + 1) + NM)$ multiplications as compared to $O(N_o N)$ in the case of direct calculation. The critical factor in the calculation is on

the requirement that one can achieve high accuracy for cases where M is much less than N .

2.3 the FMM Evaluation of the Kirchhoff Integral

In this section, we will outline how the fast multipole method can be applied to the evaluation of the Kirchhoff integral. Consider a source distribution that is enclosed in a volume V . The problem at hand is to evaluate the pressure at a spatial point located external to the volume. In such a case, the pressure can be evaluated by the volume integral

$$p(\vec{r}) = \int_V g(\vec{r}, \vec{r}_0) s(\vec{r}_0) dV_0 \quad (2.10)$$

where $p(\vec{r})$ is the pressure at the observation point \vec{r} and $s(\vec{r}_0)$ represents the source distribution in the volume V . We will assume that $|\vec{r}| > |\vec{r}_0|$ for all observation points of interest.

The source distribution $s(\vec{r}_0)$ is modeled by its samples located at N points. An element of the set of sample points is denoted as

$$s(\vec{r}_0) = \sum_{j=1}^N \delta(\vec{r}_0 - \vec{X}_j) s_j w_j \quad (2.11)$$

where, s_j is the amplitude of an individual source located at \vec{X}_j and w_j is the quadrature weight. A schematic of the problem domain is shown in Fig 2.1. This choice allows one to replace the volume integral by a summation. In the figure, the origin of the coordinate system is labeled as O . The task is to find the unknown potential at the observation point that is outside the volume enclosing the sources and Eqn (2.10) is evaluated numerically.

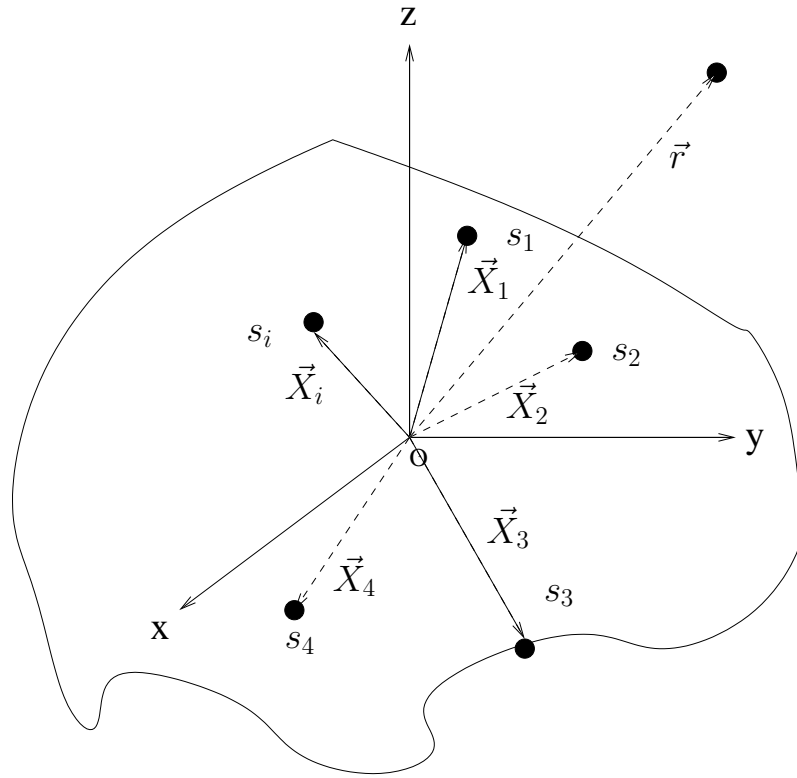


Figure 2.1: Source locations and amplitudes

$$p(\vec{r}) = \sum_{j=1}^N s_j w_j \int_v g(\vec{r}, \vec{r}_0) \delta(\vec{r}_0 - \vec{X}_j) dV_0 \quad (2.12)$$

Using the integral property of the delta function, Eqn (2.12) can be rewritten as

$$p(\vec{r}) = \sum_{j=1}^N s_j w_j g(\vec{r}, \vec{X}_j) \quad (2.13)$$

To calculate the unknown potential at the observation point in spherical coordinate system, the Green's function in Eqn (2.13) can be expressed as follows when $|\vec{r}| > |\vec{X}_j|$,

$$g(\vec{r}, \vec{X}_j) = i\gamma \sum_{n=0}^T \sum_{m=-n}^n R_n^{-m}(\vec{X}_j) S_n^m(\vec{r}) \quad (2.14)$$

Substituting Eqn (2.14) in Eqn (2.13) yields

$$p(\vec{r}) = i\gamma \sum_{n=0}^T \sum_{m=-n}^n S_n^m(\vec{r}) \sum_{j=1}^N s_j w_j R_n^{-m}(\vec{X}_j) \quad \text{if } |\vec{r}| > |\vec{X}_j| \quad (2.15)$$

The summation in the index j can be calculated separately and yields the coefficient

a_{nm} .

$$a_{nm} = \sum_{j=1}^N s_j w_j R_n^{-m}(\vec{X}_j) \quad (2.16)$$

As a result Eqn (2.15) becomes

$$p(\vec{r}) = i\gamma \sum_{n=0}^T \sum_{m=-n}^n S_n^m(\vec{r}) a_n^m \quad \text{if } |\vec{r}| > |\vec{X}_j| \quad (2.17)$$

Using Eqn (2.17) one can calculate the pressure at the observation points outside the volume enclosed by source points. The expansion in the Eqn (2.17) is referred to as the far field expansion or S-expansion.

2.4 Multipole Expansion about an Arbitrary Reference Point

In this section, we will examine how one can evaluate the multipole expansion about a prescribed reference point. Fig (2.2) shows the position of the source points, observation points and reference point P . The vector \vec{X} and \vec{d} are the position

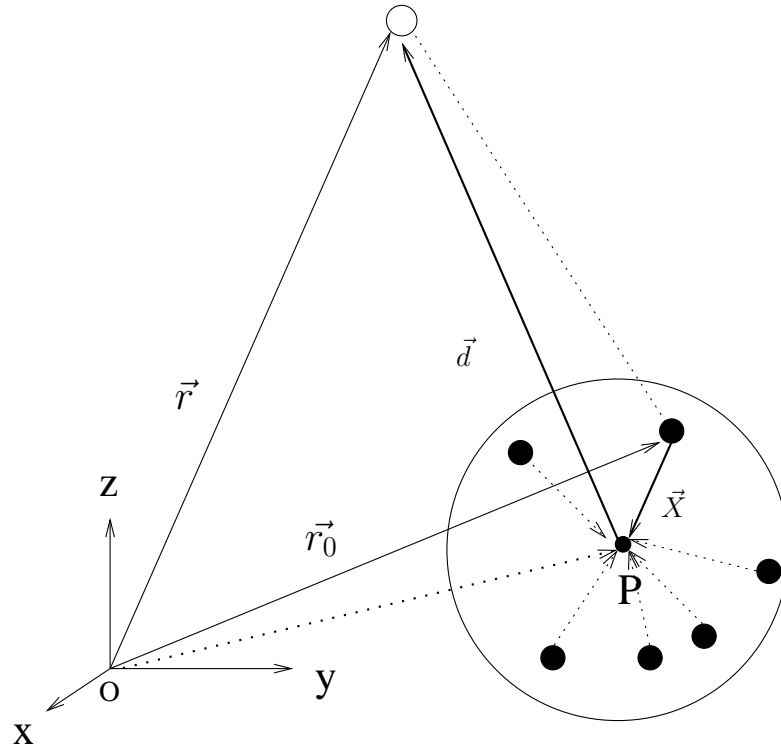


Figure 2.2: Evaluation of the potential with respect to P

vectors of the source point and observation point, respectively, with respect to P . The potential at the observation point \vec{r} is given by Eqn (1.54). The potential at the observation point will be evaluated with respect to P using Eqn (1.54).

Using the addition theorem of vectors, we can derive the relation between

position vectors \vec{r} , \vec{r}_0 and \vec{X} , \vec{d} .

$$\begin{aligned}\vec{r} - \vec{r}_0 &= \vec{X} + \vec{d} \\ &= \vec{X} - (-\vec{d})\end{aligned}\tag{2.18}$$

Substituting the aforementioned relation for $\vec{r} - \vec{r}_0$, the free space and spherical Green's function can be rewritten as

$$g(\vec{X}, -\vec{d}) = \frac{e^{ik|\vec{X}+\vec{d}|}}{4\pi|\vec{X} + \vec{d}|} \simeq \begin{cases} i\gamma \sum_{n=0}^T \sum_{m=-n}^n S_n^{-m}(\vec{X}) R_n^m(-\vec{d}), & |\vec{X}| > |\vec{d}| \\ i\gamma \sum_{n=0}^T \sum_{m=-n}^n S_n^m(-\vec{d}) R_n^{-m}(\vec{X}), & |\vec{X}| < |\vec{d}| \end{cases}\tag{2.19}$$

We will focus on the case when $|\vec{X}| < |\vec{d}|$. Eqn (2.19) can be expressed for large number of source points. Fig (2.3) shows the sources s_1, s_2, \dots, s_N with position vectors X_1, X_2, \dots, X_N . As we can see, the reference point P is geometrically located at the cluster center of the source points. The potential at the observation point \vec{r}

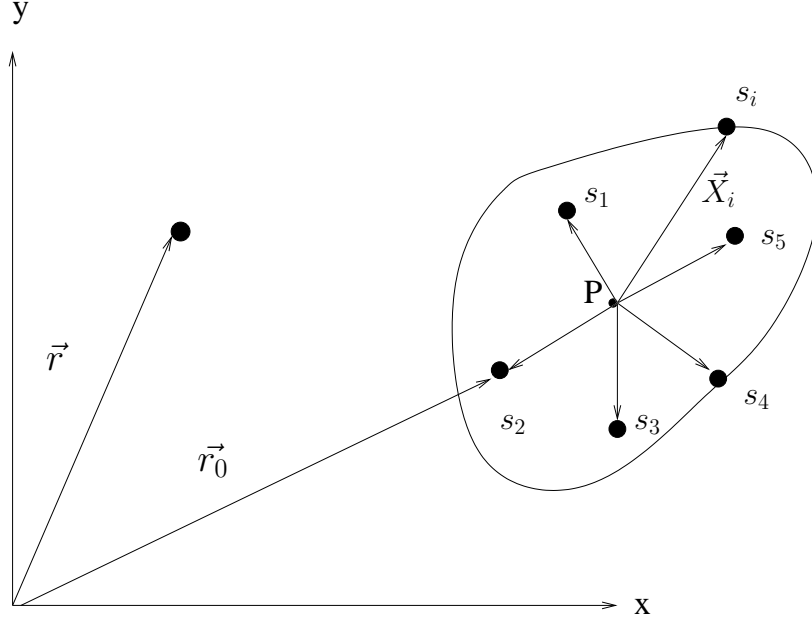


Figure 2.3: the source locations with respect to reference point

when $|\vec{d}| > |\vec{X}|$ is given by

$$p(\vec{d}) = i\gamma \sum_{j=0}^N s_j w_j \sum_{n=0}^T \sum_{m=-n}^n R_n^{-m}(\vec{X}_j) S_n^m(-\vec{d}) \quad (2.20)$$

The summation in the index j can be equated to the coefficient

$$a_{nm} = \sum_{j=0}^N R_n^{-m}(\vec{X}_j) s_j w_j \quad (2.21)$$

Substituting the above expression in Eqn (2.20) yields

$$p(\vec{d}) = i\gamma \sum_{n=0}^T \sum_{m=-n}^n a_{nm} S_n^m(-\vec{d}) \quad (2.22)$$

where N is the total number of sources close to the reference point P .

2.5 Numerical Results for the Accuracy of the Potential with the Expansion Coefficients

2.5.1 Accuracy for the Green's function

In this section, we will compare the free space Green's function $g_f(\vec{r}, \vec{X})$ to the spherical Green's function $g_s(\vec{r}, \vec{X})$ which is calculated using expansion coefficients.

$$g_f(\vec{r}, \vec{X}) = \frac{e^{i\gamma|\vec{r}-\vec{X}|}}{4\pi|\vec{r}-\vec{X}|} \quad (2.23)$$

$$g_s(\vec{r}, \vec{X}) = i\gamma \sum_{n=0}^T \sum_{m=-n}^n R_n^{-m}(\vec{X}) S_n^m(\vec{r}) \quad (2.24)$$

The development of the problem is as follows. The observation grid is considered as $1 \leq x \leq 41$, $1 \leq y \leq 41$, $z = 0$ and the source is located on $(10, 10, 0)$. The total number of grid points are 100 including the source point. Green's function is calculated for all the points with distance more than the distance of the source point from the origin of the coordinate system. In this case, the function is calculated for the all the points with distance more than $\sqrt{10^2 + 10^2} = 14.14$ and $\gamma = 1$. For the Eqn (2.24) truncation order chosen is 47.

Contour plots are used to demonstrate the numerical results as shown in Fig (2.4). Lines show the magnitude of $g_f(\vec{r}, \vec{X})$ and points show the magnitude of $g_s(\vec{r}, \vec{X})$. Ideally, each set of points should follow the corresponding lines in the Fig (2.4). The largest error occurs at $(10, 10, 0)$ as can be seen in Fig (2.4). The results show that free space and spherical Green's function are approximately equal.

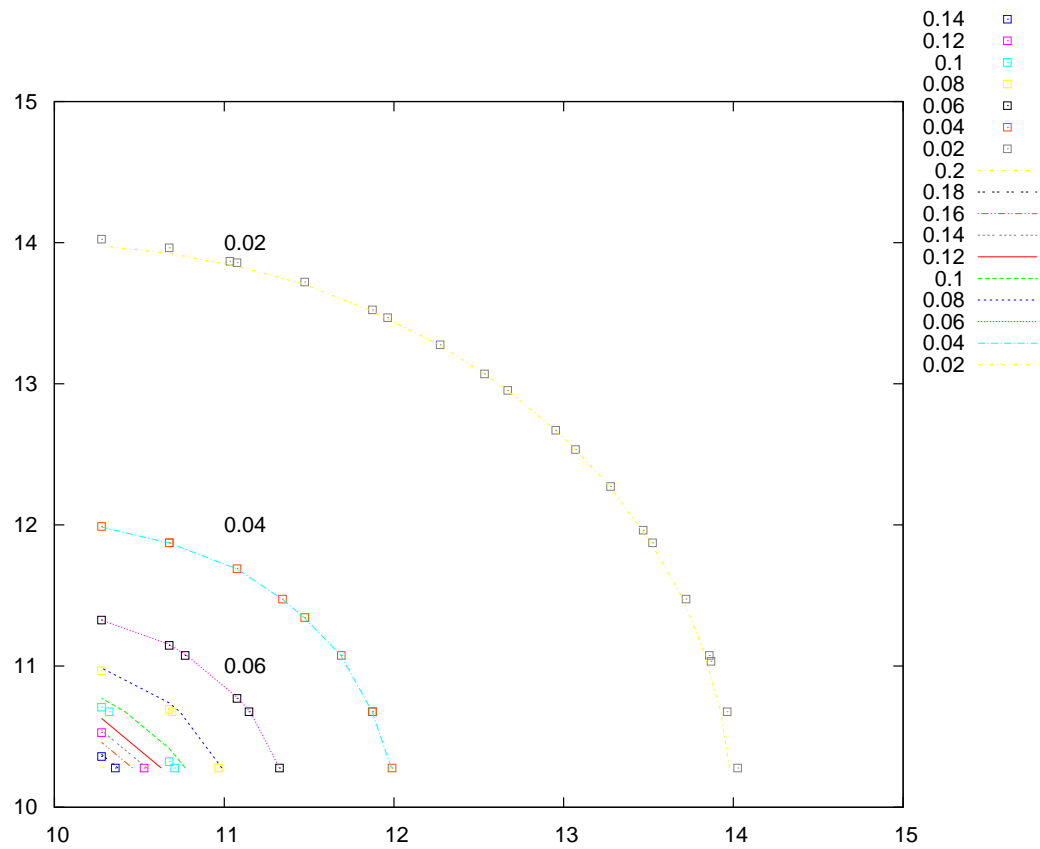


Figure 2.4: Error Analysis for the Green's function

2.5.2 Approximation Error for the Potential with the Expansion Coefficients

Consider comparing the potential calculated with the free space Green's function $p_f(\vec{r})$ to the potential calculated with the expansion coefficients $p_s(\vec{r})$ for the multipole source case. The potential at the observation point using free space Green's function is given by

$$p_f(\vec{r}) = \sum_{i=0}^N s_i \frac{e^{i\gamma|\vec{r}-\vec{X}_i|}}{4\pi|\vec{r}-\vec{X}_i|} \quad (2.25)$$

The potential at the observation point using the expansion coefficients is given by (using Eqns (2.20 to 2.22))

$$p_s(\vec{r}) = i\gamma \sum_{n=0}^T \sum_{m=-n}^n a_{nm} S_n^m(\vec{r}) \quad (2.26)$$

where

$$a_{nm} = \sum_{i=j}^N s_j R_n^{-m}(\vec{X}_j) \quad (2.27)$$

For the numerical results, we will use Eqns (2.25 and 2.26). The observation grid is considered as $1 \leq x \leq 41$, $1 \leq y \leq 41$ and $z = 0$. The total number of points chosen are 100 including source points. Four source points are chosen, location of the each source is $s_1 = (10, 10, 0)$, $s_2 = (-5, -5, 0)$, $s_3 = (2, 2, 0)$, $s_4 = (-2, -2, 0)$ and the magnitude of the each source is 1. To calculate $p_s(\vec{r})$ the truncation order chosen is 35. First the coefficients are calculated for each source and these coefficients are used to calculate the potential $p_s(\vec{r})$ using Eqn (2.26). In this case, the potential is calculated for all the points with distance more than $\sqrt{10^2 + 10^2} = 14.14$ and $\gamma = 1$.

The results are plotted in Fig (2.5) and contour plots are used to demonstrate the results. In Fig (2.5), lines show the magnitude of $p_f(\vec{r})$ and points show the magnitude of $p_s(\vec{r})$. Ideally, each set of points should follow the corresponding lines in the Fig (2.5). Largest error occurs at $(10, 10, 0)$ as can be seen in Fig (2.5). The error decreases with the increasing distance from the source point. Results show that potential calculated with the expansion coefficients is a good approximation.

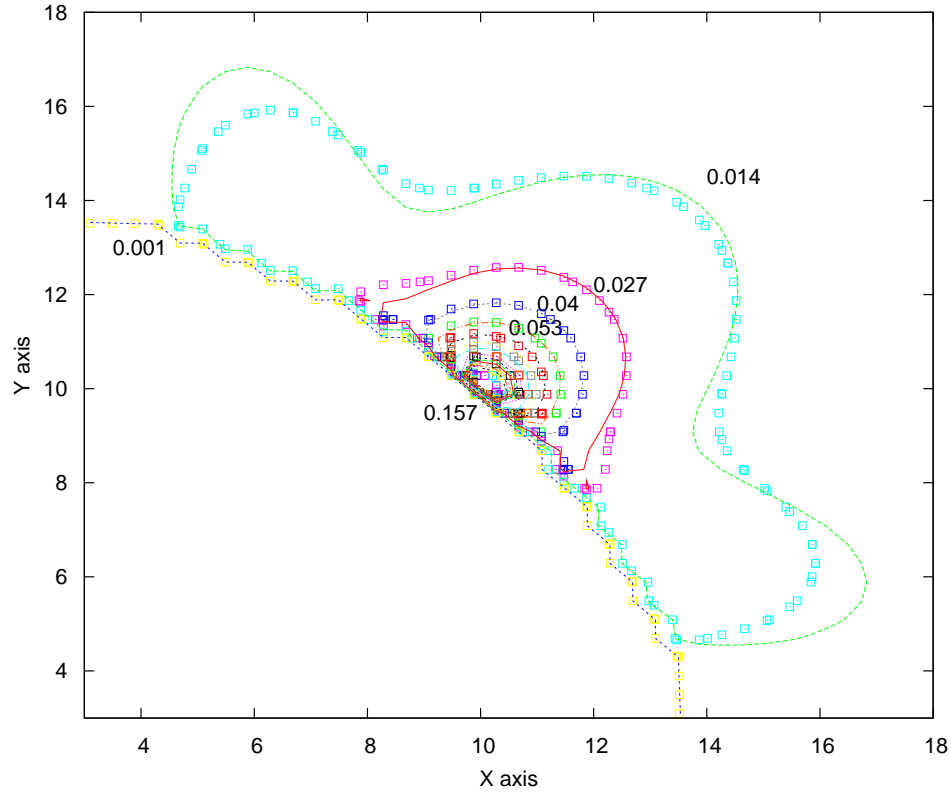


Figure 2.5: Error analysis for the potential

CHAPTER 3

TRANSLATION ERROR ANALYSIS FOR SINGLE LEVEL FAST MULTIPOLE METHOD(SLFMM)

3.1 Introduction

In this chapter, a translation error analysis is developed for the single level fast multipole method (SLFMM). In SLFMM, the computational domain is subdivided into subdomains [18]. The objective is to speed up the calculation. However when using the subdomain method the translation coefficients must be calculated. These coefficients can be a source of numerical error when the inter-subdomain distance is small.

3.2 Translation Coefficients

Consider the case where the computational domain D is subdivided into K subdomains each containing sources as shown in Fig 3.1. Each subdomain will be labeled as D_k where subscript k denotes the domain index. Domain D is the union of all the D_k for $k = (1 : K)$. The reference position in subdomain D_k is labeled P_k , following the convention given in Chapter 3.

The contribution of the sources in subdomain D_k to potential at point Q in

subdomain D_Q is equal to

$$\sum_{n=0}^{\infty} \sum_{m=-n}^n A_n^m(k) S_n^m(\vec{r}_k) \quad (3.1)$$

where $A_n^m(k)$ are coefficients that reflect the source contributions from D_k .

The potential ϕ at \vec{r}_Q is the superposition of the potential of each domain.

$$\phi(\vec{r}_Q) = \phi_Q + \sum_{\substack{k=1 \\ k \neq Q}}^K \sum_{n=0}^{\infty} \sum_{m=-n}^n A_n^m(k) S_n^m(\vec{r}_k) \quad (3.2)$$

where ϕ_Q is the result of self-excitation in domain D_Q and must be computed separately. The vector distance from the reference point P_k to the observation is

$\vec{r}_k = \vec{r}_{kQ} + \vec{r}_Q$ where $\vec{r}_{kQ} = \vec{P}_Q - \vec{P}_k$. Therefore the potential can be rewritten as

$$\phi(\vec{r}_Q) = \phi_Q + \sum_{\substack{k=1 \\ k \neq Q}}^K \sum_{n=0}^{\infty} \sum_{m=-n}^n A_n^m(k) S_n^m(\vec{r}_{kQ} + \vec{r}_Q) \quad (3.3)$$

Each singular function S_n^m is translated by the vector distance \vec{r}_{kQ} in Eqn (3.3). The singular function can be expanded in two regions, $|\vec{r}_{kQ}| > |\vec{r}_Q|$ and $|\vec{r}_{kQ}| < |\vec{r}_Q|$. If $|\vec{r}_{kQ}| > |\vec{r}_Q|$ for all values of the index $k \neq Q$ one can express

$$S_n^m(\vec{r}_{kQ} + \vec{r}_Q) = \sum_{l=0}^{\infty} \sum_{s=-l}^l [(S|R)_{ln}^{sm}(\vec{r}_{kQ})] R_l^s(\vec{r}_Q) \quad (3.4)$$

where [35]

$$[(S|R)_{ln}^{sm}(\vec{r}_{kQ})] = \sum_{\alpha=0}^{\infty} \sum_{\beta=-\alpha}^{\alpha} S_{\alpha}^{\beta}(\vec{r}_{kQ}) (S|r)_{\alpha ln}^{\beta sm} \quad (3.5)$$

The coefficient $S|r_{\alpha ln}^{\beta sm}$ can be expressed as

$$(S|r)_{\alpha ln}^{\beta sm} = i^{l-n+\alpha} (4\pi) \int_{-\pi}^{\pi} d\phi \int_0^{\pi} Y_n^m Y_l^{-s} Y_{\alpha}^{-\beta} \sin(\theta) d\theta \quad (3.6)$$

By virtue of orthogonality of the spherical harmonics

$$(S|r)_{\alpha ln}^{\beta sm} = \begin{cases} i^{(l-n-\alpha)} \frac{4\pi}{\sqrt{2\pi}} \int_{-1}^1 P_n^{|m|} P_l^{|s|} P_{\alpha}^{|\beta|} d\eta & \text{if } \alpha \geq |\beta|; \beta = m - s \\ 0 & \text{otherwise} \end{cases} \quad (3.7)$$

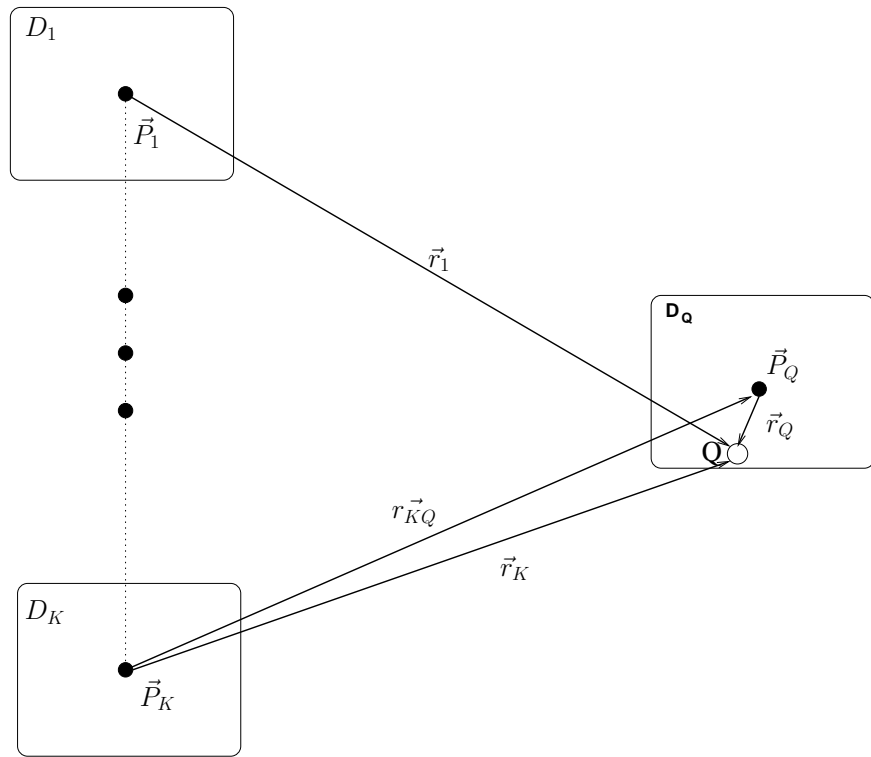


Figure 3.1: Evaluation of the potential at \vec{r}_Q where $|\vec{r}_Q| < |\vec{r}_{QK}|$

and $\zeta = \cos(\theta)$.

Similarly, if $|\vec{r}_{kQ}| < |\vec{r}_Q|$ for all values of the index $k \neq Q$ as shown in Fig (3.2)

one can express

$$S_n^m(\vec{r}_{kQ} + \vec{r}_Q) = \sum_{l=0}^{\infty} \sum_{s=-l}^l [(S|S)_{ln}^{sm}(\vec{r}_{kQ})] S_l^s(\vec{r}_Q) \quad (3.8)$$

where [35]

$$[(S|S)_{ln}^{sm}(\vec{r}_{kQ})] = \sum_{\alpha=0}^{\infty} \sum_{\beta=-\alpha}^{\alpha} S_{\alpha}^{\beta}(\vec{r}_{kQ})(S|s)_{\alpha ln}^{\beta sm} \quad (3.9)$$

The coefficient $(S|s)_{\alpha ln}^{\beta sm}$ can be expressed as

$$(S|s)_{\alpha ln}^{\beta sm} = i^{\alpha-n+l} (4\pi) \int_{-\pi}^{\pi} d\phi \int_0^{\pi} Y_n^m Y_l^{-s} Y_{\alpha}^{-\beta} \sin(\theta) d\theta \quad (3.10)$$

By virtue of orthogonality of the spherical harmonics

$$(S|s)_{\alpha ln}^{\beta sm} = \begin{cases} i^{(\alpha-n+l)} \frac{4\pi}{\sqrt{2\pi}} \int_{-1}^1 P_n^{|m|} P_l^{|s|} P_{\alpha}^{|\beta|} d\eta & \text{if } \alpha > |\beta|; \beta = m - s \\ 0 & \text{otherwise} \end{cases} \quad (3.11)$$

and $\eta = \cos(\theta)$. As we can see from Eqns (3.7 and 3.11), the calculation of coefficients $(S|r)_{\alpha ln}^{\beta sm}$ and $(S|s)_{\alpha ln}^{\beta sm}$ require three orders. The translation coefficients are calculated using the addition theorem as in Eqns (3.5 and 3.9). The calculation of the translation coefficient given in Eqn (3.8) is a non-recurring cost. Therefore it is an efficient method for large number of particles.

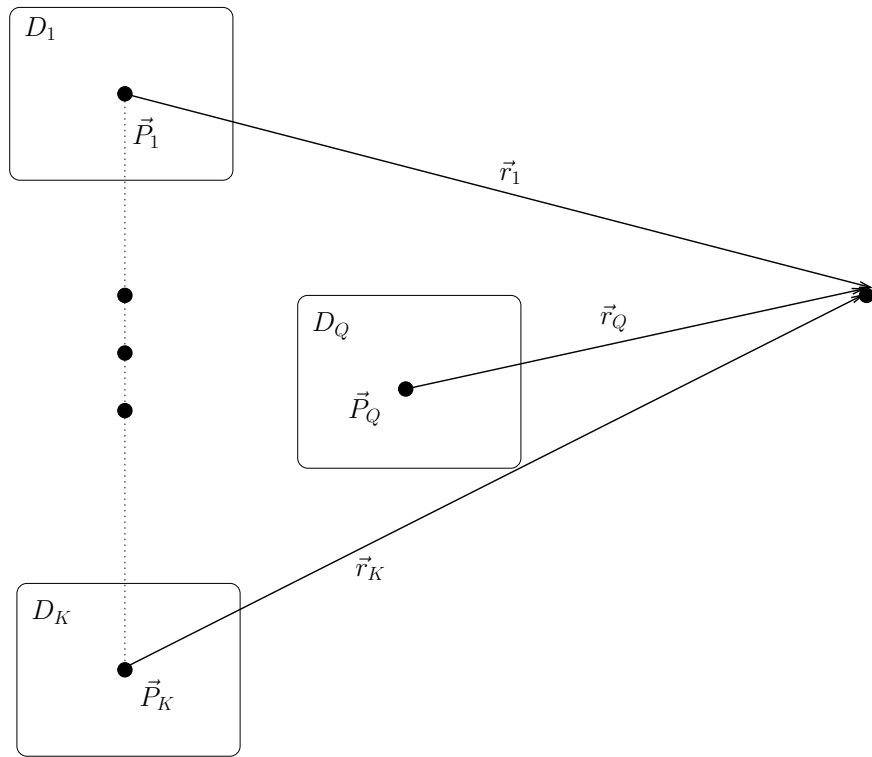


Figure 3.2: Evaluation of the potential at \vec{r}_Q where $|\vec{r}_Q| > |\vec{r}_{QK}|$

3.3 Translation Error Analysis for the Green's Function

In this section, we will analyze the translation error for the Green's function. The error analysis compares the Green's function calculated using the translation method and the Green's function calculated using the direct method. In the translation method, the level of truncation of the series plays an important role in the convergence rate of the Green's function. Therefore, we will analyze translation error with respect to the truncation order.

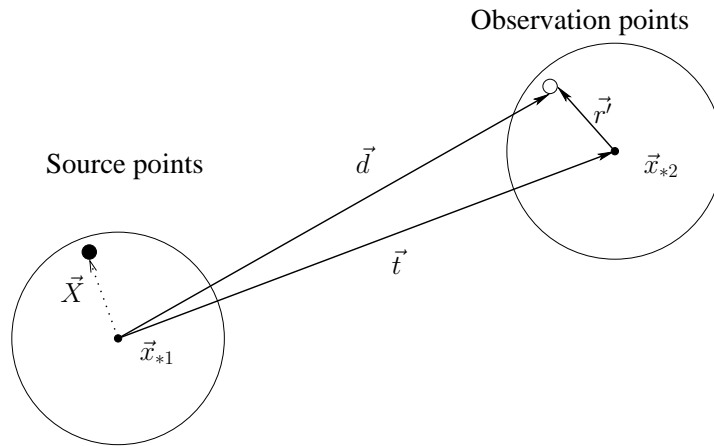


Figure 3.3: Vector representation for translation method

Expression for the Green's function using exact, direct and translation method can be given with reference to Fig (3.3) as follows. In Fig (3.3), \vec{x}_{*1} and \vec{x}_{*2} are reference points for source and observation points respectively. \vec{X} , \vec{d} are the locations of the source point and observation point respectively with respect to reference point \vec{x}_{*1} , \vec{r} is the distance of observation point from \vec{x}_{*2} and \vec{t} is translation vector between \vec{x}_{*1} and \vec{x}_{*2} . Using vector addition $\vec{d} = \vec{t} + \vec{r}$, the expression for the exact Green's

function is given by (from 2.19)

$$g_f(\vec{X}, \vec{d}) = \frac{e^{ik|\vec{X}+\vec{d}|}}{4\pi|\vec{X} + \vec{d}|} \quad (3.12)$$

The expression for the Green's function with the direct method is given by

$$g_s(\vec{X}, \vec{d}) = i\gamma \sum_{n=0}^T \sum_{m=-n}^n R_n^{-m}(\vec{X}) S_n^m(\vec{d}) \quad \text{if } |\vec{d}| > |\vec{X}| \quad (3.13)$$

The expression for the Green's function using the translation method is given by

substituting $\vec{d} = \vec{t} + \vec{r}'$. The expression for the Green's function is rewritten for $|\vec{t}| > |\vec{r}'|$

$$g_t(\vec{X}, \vec{t} + \vec{r}') = i\gamma \left\{ \begin{aligned} & \sum_{n=0}^T \sum_{m=-n}^n R_n^{-m}(\vec{X}) S_n^m(\vec{t} + \vec{r}') \\ & \sum_{n=0}^T \sum_{m=-n}^n R_n^{-m}(\vec{X}) \sum_{l=0}^{\hat{L}} \sum_{s=-l}^l [(S|R)_{ln}^{sm}(\vec{t})] R_l^s(\vec{r}') \\ & \sum_{n=0}^T \sum_{m=-n}^n R_n^{-m}(\vec{X}) \{ \sum_{l=0}^{\hat{L}} \sum_{s=-l}^l \sum_{\alpha=0}^{\hat{P}} \sum_{\beta=-\alpha}^{\alpha} S_{\alpha ln}^{\beta sm} S_{\alpha}^{\beta}(\vec{t}) R_l^s(\vec{r}') \} \end{aligned} \right. \quad (3.14)$$

where T, \hat{L} and \hat{P} are the truncation orders. Relative error for the Green's function with the direct method is given by $|\frac{(g_f - g_s)}{g_f}|$ and with the translation method is given by $|\frac{(g_f - g_t)}{g_f}|$. Using Eqns ((3.12) – (3.14)), we will calculate the Green's functions and plot the results for relative error. For the numerical results, the following example is demonstrated in the next section.

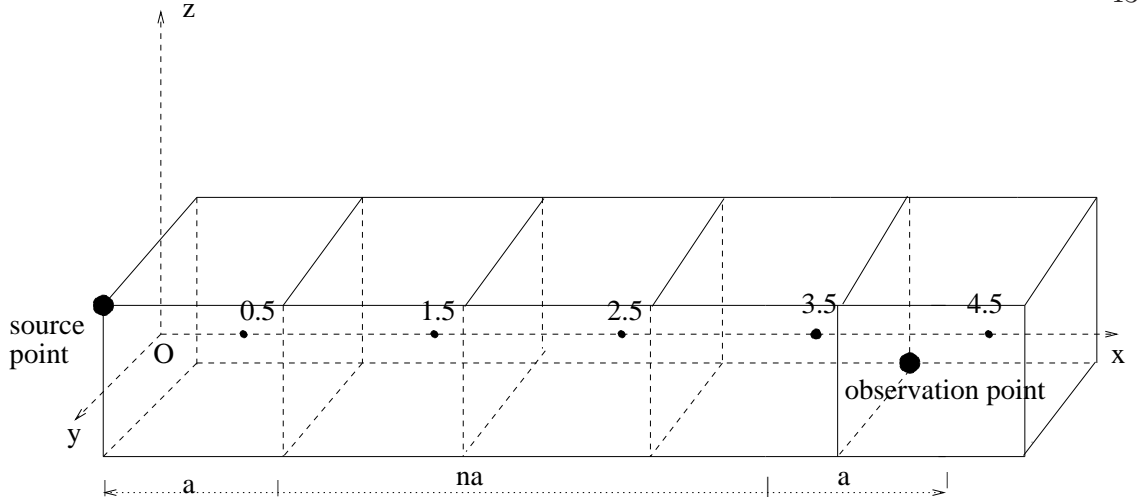


Figure 3.4: Error analysis for cube shape

3.4 Translation Error analysis for the cubically shaped subdomains

Five cubes of the side $a = 1$ are clustered as shown in Fig (3.4). The origin of the coordinate system is at O . The number of cubes between the first and last cubes is n , also referred to as the number of buffer boxes. The distance between the centers of the two end cubes is $(n + 1)a$. Centers of the cubes are located at locations 0.5, 1.5, 2.5, 3.5, 4.5 on the x axis. The source is located at $(0, 0.5, 0.5)$ and observation point is at $(4, -0.5, -0.5)$. The reference point is at $(0.5, 0, 0)$. Therefore the coordinates for source and observation points with reference to Figs (3.3 and 3.4) are $\vec{X} = (0.5, -0.5, -0.5)$, $\vec{d} = (-3.5, 0.5, 0.5)$, $\vec{x}_{*1} = (0.5, 0, 0)$, $\vec{x}_{*2} = (4.5, 0, 0)$, $\vec{t} = (3, 0, 0)$, $\vec{r} = (0.5, -0.5, -0.5)$. In our analysis the wavenumber is fixed to $k = 2\pi$ and $ka = 2\pi$.

Translation error analysis is demonstrated for the problem geometry as shown in Fig (3.4). Relative error calculated with $|\frac{(g_f - g_s)}{g_f}|$ referred to as direct method is

compared with relative error calculated with $|\frac{(g_f - g_t)}{g_f}|$ referred to as the translation method. g_f , g_s and g_t are calculated using Eqn(3.12), Eqn(3.13) and Eqn(3.14) respectively. The relative error is analyzed for two cases of the buffer boxes 1 and 5. The estimated error is calculated using

$$digits \simeq \left[\frac{T - k\sqrt{X}}{1.8(k\sqrt{X})^{\frac{1}{3}}} \right]^{\frac{3}{2}} \quad (3.15)$$

$$estimated \ error \simeq 10.0^{-digits} \quad (3.16)$$

where k is the wavenumber and X is the distance of the source from the reference point of the source domain. The results for the relative error versus truncation order are plotted in Fig(3.5). The x-axis and y-axis are labeled as truncation order and the relative error respectively. The results are plotted with the lines and respective labels for the different methods and buffer boxes are as shown in the Fig(3.4).

The results show that the estimated error decreases with the increasing truncation number. For the buffer box 5, the relative error for both the direct and translation method decreases with the order and respective lines coincide with each other at certain locations. Minimum computed error in our simulation was 10^{-6} . This level was reached for buffer box 5 with the translation method and the direct method. At truncation order 16 the round-off error dominates for both the translation and direct methods. Above the truncation order 16, the relative error is independent of the truncation order.

For the buffer box 1, with the direct method the relative error decreases with the truncation order and around truncation order 17 the round-off error dominates. With the translation method, the relative error diverges at the truncation order 12

and minimum error is 0.001. The divergence occurs due to the Bessel function of the second kind when the order is greater than the argument, which is explained in the next section. Due to the divergence of the function, truncation order can not be selected and error is independent of the truncation order.

We see that for the buffer box 1 the translation and direct methods are in agreement for truncation order less than 12. However, the error in a translation method increases for higher truncation order. The argument of the second kind Bessel function is an important parameter for the application of the translation method. The argument is the distance between the centers of the source domain and observation domain. Therefore, the distance between centers of domains puts the limitation on the translation method and it can not be used for the observation points in the neighborhood of the source domain. In this problem the wavelength is equal to the box size. Therefore translation method fails if the distance between the centers of the two subdomains is equal to the wavelength.

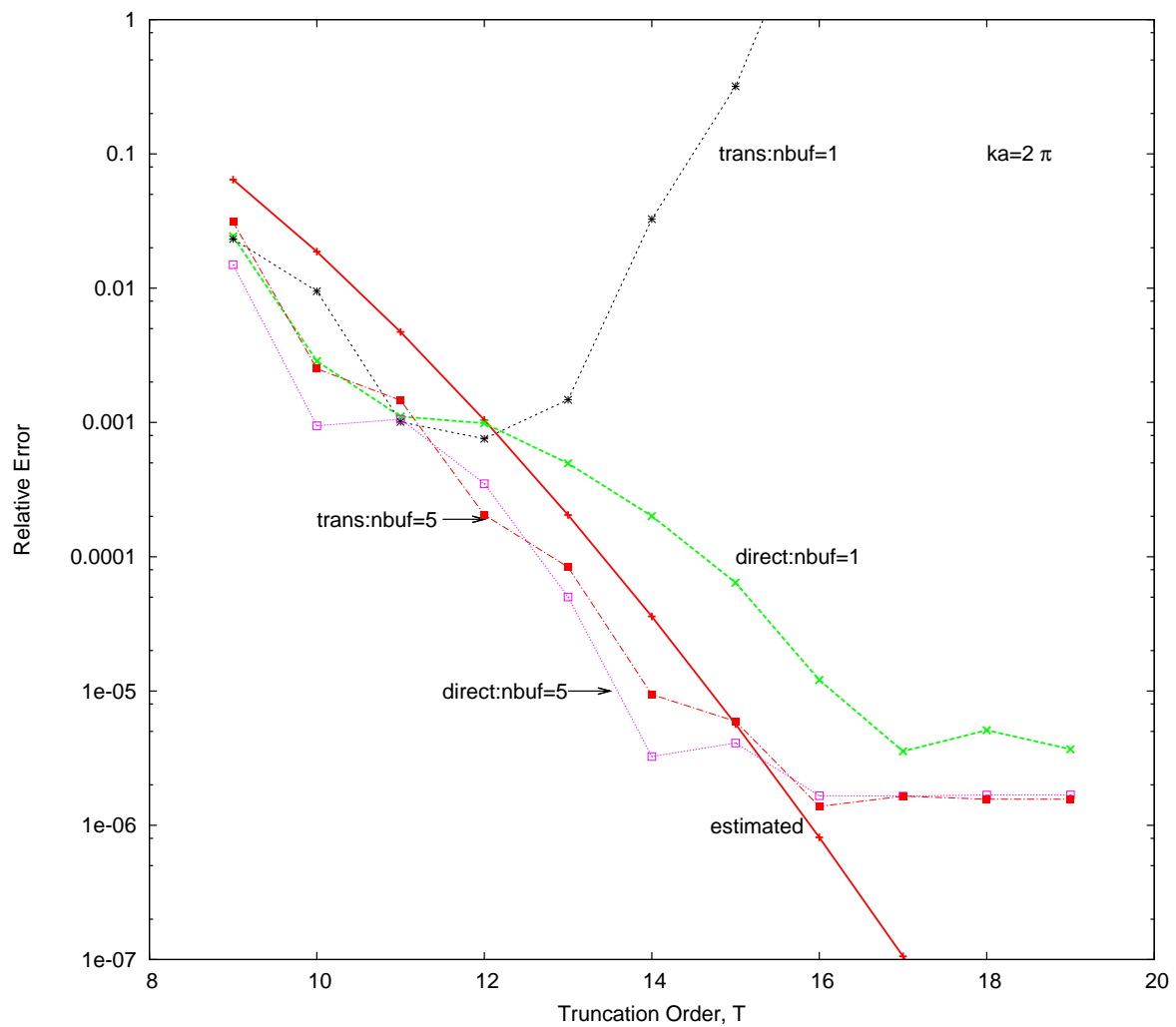


Figure 3.5: Relative error versus truncation order for cubically shaped subdomains

3.5 Hankel function and Divergence of the Green's function

In this section, we will see Hankel function and explain how imaginary part of the Hankel function contributes to the divergence of the Green's function. The Green's function is given by [17] [36]

$$\begin{aligned} g(\vec{X}, \vec{d}) &= \frac{e^{ik|\vec{X}+\vec{d}|}}{4\pi|\vec{X}+\vec{d}|} \\ &= \frac{ik}{4\pi} \sum_{n=0}^T (-1)^n (2n+1) j_n(kX) h_n^1(kd) P_n(\hat{X} \cdot \hat{d}) \end{aligned} \quad (3.17)$$

The expression for the Green's function consist of the spherical Bessel function of the first kind j_n , spherical Hankel function of first kind h_n^1 and Legendre polynomial P_n . \vec{X} and \vec{d} are the position vectors for source point and observation point respectively from some reference point. \hat{X} and \hat{d} are their unit vectors.

The divergence of the Green's function is due to the Hankel function which is explained as follows. Expression for Hankel function is $h_n(kd) = j_n(kd) + iy_n(kd)$. As $\lim_{d \rightarrow 0} j(kd)$ then $j_n(kd)$ approaches towards unity and when $\lim_{d \rightarrow 0} y(kd)$ then $y_n(kd)$ approaches infinity. When the argument of the imaginary part of the spherical Hankel function of the first kind goes to 0 it moves towards infinity [17]. If the argument of $y_n(kd)$ is large, then the function converges in that region. If the argument is small and order is high, then function diverges. Therefore when kd is small and order is high then the Green's function diverges. The order is directly proportional to the size of the cluster of points. The Bessel function of the first order is convergent but the second order is divergent.

Asymptotic behavior for the Bessel function of second kind is studied in this

section. Asymptotic form of ordinary Bessel functions J and Y are [37]

$$J_\alpha(z) \sim \frac{1}{\Gamma(\alpha+1)} \left(\frac{z}{2}\right)^\alpha \quad (3.18)$$

and

$$Y_\alpha(z) \sim \frac{-\Gamma(\alpha)}{\pi} \left(\frac{2}{z}\right)^\alpha \quad (3.19)$$

The relation between the ordinary and spherical Bessel function is given by

$$j_n(x) = \sqrt{\frac{\pi}{2x}} J_{n+\frac{1}{2}}(x) \quad (3.20)$$

and

$$y_n(x) = \sqrt{\frac{\pi}{2x}} Y_{n+\frac{1}{2}}(x) \quad (3.21)$$

The asymptotic behavior for the spherical Bessel functions can be given by expressing

Eqns (3.20 and 3.21) in terms of Eqns (3.18 and 3.19)

$$j_n(x) = \sqrt{\frac{\pi}{x}} \frac{1}{\Gamma(n+\frac{3}{2})} \left(\frac{x}{2}\right)^{n+1/2} \quad (3.22)$$

and

$$y_n(x) = - \sqrt{\frac{\pi}{2x}} \frac{\Gamma(n+\frac{1}{2})}{\pi} \left(\frac{2}{x}\right)^{n+1/2} \quad (3.23)$$

In the Eqn (3.17) solving the product as

$$j_n(kX)h_n^1(kd) = j_n(kX) [j_n(kd) + iy_n(kd)] \quad (3.24)$$

The imaginary part of the Eqn (3.24) has singularity when the argument goes to 0.

$$j_n(kX)iy_n(kd) = - \frac{i}{2kd} \frac{\Gamma(n+\frac{1}{2})}{\Gamma(n+\frac{3}{2})} \left(\frac{X}{d}\right)^n \quad (3.25)$$

In Eqn (3.25) d is in the denominator for the imaginary part of the Hankel function resulting in the divergence of the Green's function when $\lim_{d \rightarrow 0}$.

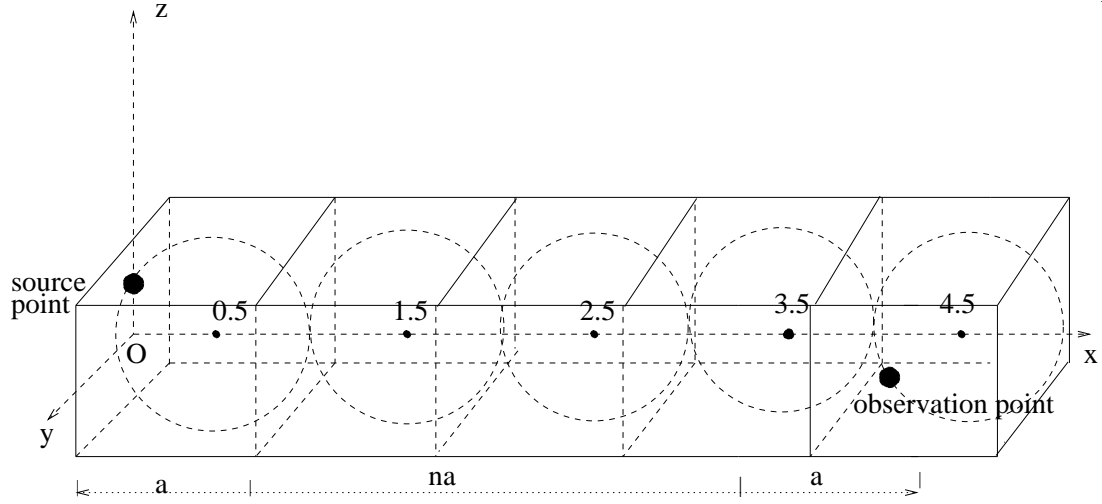


Figure 3.6: Error analysis for sphere shape cluster

3.6 Translation Error analysis for the spherically shaped subdomains

In this section, a truncation error analysis is performed for the spherically shaped subdomains. The problem geometry considered is shown in Fig (3.6). Five spheres are clustered together and centers of spheres are 0.5, 1.5, 2.5, 3.5, 4.5. The source location is at $(0, 0.3535, 0.3535)$. The observation point is at $(-2, -0.3535, -0.3535)$ when the buffer box is 1 and $(-4, -0.3535, -0.3535)$ when the buffer box is 4. The truncation error is analyzed for varying buffer boxes. In our analysis, the wavenumber is fixed to $k = 2\pi$.

The results of our calculations are shown in Fig (3.7). The magnitude of the relative error is plotted versus truncation order. The results for the buffer boxes (1, 5, 20, 40, 100) are shown. The relative error is calculated for the Green's function with the direct method and the translation method. For the direct method, the minimum error is approximately equal to 10^{-6} . In the translation method, the error

varies with the number of buffer boxes as well as truncation order. With the buffer box 1 the error is equal to 10^{-4} which is one order of a magnitude lower than in the cubically shaped subdomains case. However, the error increases for the higher truncation orders. For the buffer boxes (5, 20, 40, 100) the relative error decreases for both direct and translation method but the round-off error increases with the increase in buffer boxes.

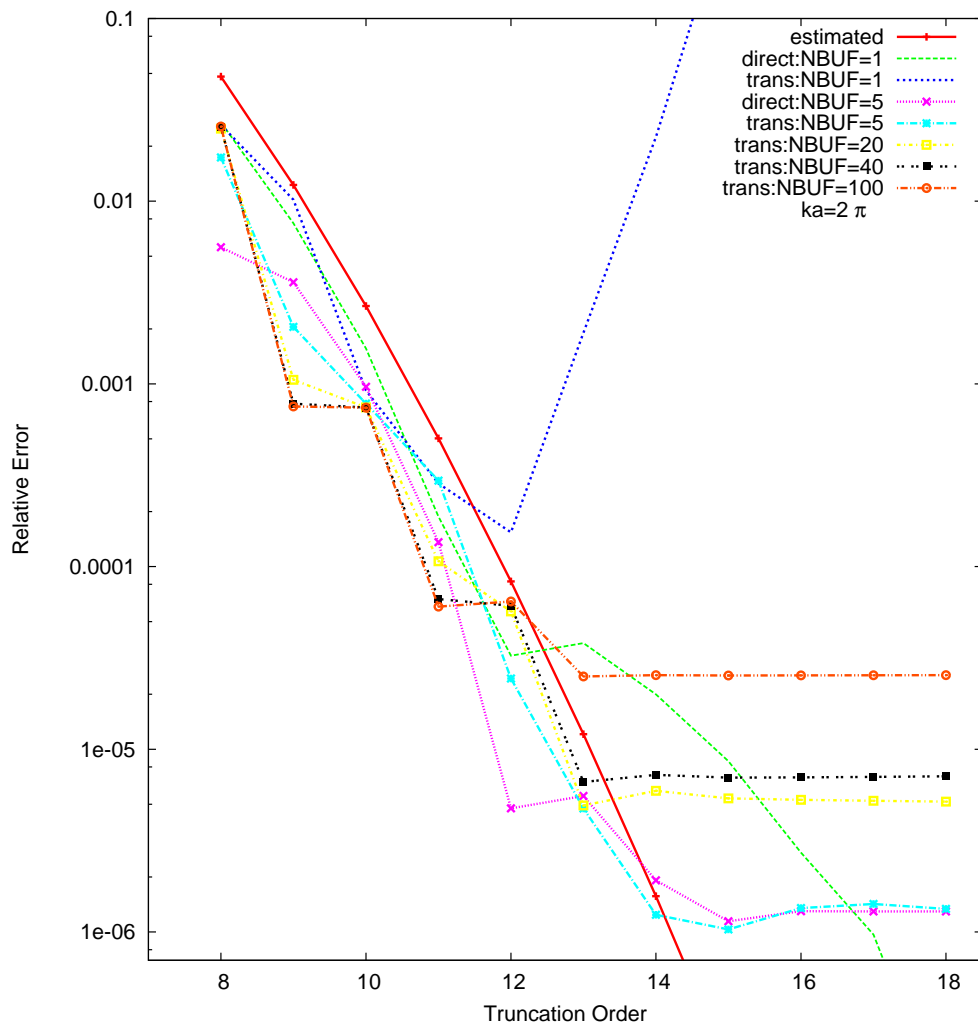


Figure 3.7: Translation error analysis for spherically shaped subdomains with different buffer boxes

3.7 Conclusion

We examined translation method with respect to the truncation order. It is an efficient method as it is non-recurring cost but has limitations due to the truncation order. The observation domain can not be close to the source domain due to divergence. Also numerical computation contributes to the inefficiency of the translation method as it introduces the round-off error.

Appendices

APPENDIX 1

DERIVATION OF THE SOLUTION TO THE HELMHOLTZ WAVE EQUATION IN SPHERICAL COORDINATE SYSTEM

The Helmholtz equation in spherical coordinate system is given as follows [4].

$$\frac{1}{r^2} \frac{\partial}{\partial r} \left(r^2 \frac{\partial g}{\partial r} \right) + \frac{1}{r^2 \sin(\theta)} \frac{\partial}{\partial \theta} \left(\sin(\theta) \frac{\partial g}{\partial \theta} \right) + \frac{1}{r^2 \sin^2(\theta)} \frac{\partial^2 g}{\partial \phi^2} + k^2 g = 0 \quad (1.1)$$

To solve the Helmholtz equation we are using separation of variables method. In this method we assume the solution of the equation with respect to different variables. In this case we are assuming the solution for g as $R(r)\Theta(\theta)\Phi(\phi)$. Where $R(r)$ is the solution of the above equation with respect to variable (r) which depends on the radial distance, $\Theta(\theta)$ is the solution with respect to angle θ and $\Phi(\phi)$ is the solution with respect to variable (ϕ) which depends on the angle ϕ .

$$g(r, \theta, \phi) = R(r)\Theta(\theta)\Phi(\phi) \quad (1.2)$$

Substituting Eq (1.2) in Eqn (1.1) yields

$$\frac{1}{r^2} \frac{\partial}{\partial r} (r^2 R' \Theta \Phi) + \frac{1}{r^2 \sin(\theta)} \frac{\partial}{\partial \theta} (\sin(\theta) R \Theta' \Phi) + \frac{1}{r^2 \sin^2(\theta)} (R \Theta \Phi'') + k^2 (R \Theta \Phi) = 0 \quad (1.3)$$

Dividing Eqn (1.3) by $R\Theta\Phi$ and multiplying with $r^2 \sin^2(\theta)$ yields

$$\frac{\sin^2(\theta)}{R} \frac{\partial}{\partial r} (r^2 R') + \frac{\sin(\theta)}{\Theta} \frac{\partial}{\partial \theta} (\sin(\theta) \Theta') + \frac{\Phi''}{\Phi} + k^2 r^2 \sin^2(\theta) = 0 \quad (1.4)$$

Substituting $\frac{\Phi''}{\phi} = -m^2$ and dividing by $\sin^2(\theta)$ where m is the degree.

$$\frac{1}{R} \frac{\partial}{\partial r}(r^2 R') + \frac{1}{\Theta \sin(\theta)} \frac{\partial}{\partial \theta} \sin(\theta) \Theta' - \frac{m^2}{\sin^2(\theta)} + k^2 r^2 = 0 \quad (1.5)$$

In Eqn (1.5) replacing the terms which are dependent on θ with the following expression

$$\frac{1}{\Theta \sin(\theta)} \frac{\partial}{\partial \theta} \sin(\theta) \Theta' - \frac{m^2}{\sin^2(\theta)} = -n(n+1) \quad (1.6)$$

To solve Eqn (1.6) substitute $n = \cos(\theta)$.

Therefore $\frac{\partial n}{\partial \theta} = -\sin(\theta)$, $\sin(\theta) = \sqrt{1-n^2}$ and $\frac{\partial}{\partial \theta} = \frac{\partial n}{\partial \theta} \frac{\partial}{\partial n}$

Substituting above expressions in Eqn (1.6) gives

$$\frac{1}{\Theta \sqrt{1-n^2}} \frac{\partial n}{\partial \theta} \frac{\partial}{\partial n} (\sin(\theta) \Theta') - \frac{m^2}{(1-n^2)} = 0 \quad (1.7)$$

Solving the above equation gives

$$\frac{1}{\Theta} \frac{\partial}{\partial n} \left[(1-n^2) \frac{\partial}{\partial n} \right] - \frac{m^2 \Theta}{(1-n^2)} = 0 \quad (1.8)$$

Applying the product rule for partial derivative and multiplying by Θ gives

$$(1-n^2) \Theta'' - 2n \Theta' - \frac{m^2}{(1-n^2)} = 0 \quad (1.9)$$

Second order partial differential equation of type Eqn (1.9) is referred to as Legendre differential equation. This is the standard Eqn. and the solution to it is Legendre polynomials denoted by P_n^m , where m is the degree and n is the order.

Next we will derive the expression for the solution $R(r)$. Reconsider the Eqn (1.5) and Eqn (1.6) yields

$$\frac{1}{R} \frac{\partial}{\partial r}(r^2 R') - n(n+1) + k^2 r^2 = 0 \quad (1.10)$$

which becomes

$$r^2 R'' + 2rR' + [k^2 r^2 - n(n+1)]R = 0 \quad (1.11)$$

This is the standard Bessel's differential equation and the solution to it is the Bessel's functions of first kind $j_n(kr)$, second kind $y_n(kr)$ and Hankel function $h_n(kr)$. Therefore the solution $R(r) = J_n(kr)$ or $h_n(kr)$ depending on the location of the observation point with distance r from reference point. k is the wavenumber.

Next, we will solve for the solution with respect to angle ϕ which is $\Phi(\phi)$. In Eqn (1.4) we substituted

$$\frac{\Phi''}{\phi} = -m^2 \quad (1.12)$$

It can be rewritten as

$$\frac{1}{\phi} \frac{\partial^2 \Phi(\phi)}{\partial \phi^2} = -m^2 \quad (1.13)$$

which results in a standard second order differential equation and solution to it from [38] is

$$\Phi(\phi) = Ae^{-im\phi} + Be^{im\phi} \quad (1.14)$$

where A and B are constants.

APPENDIX 2

VARIETY OF SPECIAL FUNCTIONS

A variety of functions appear in the solution of the Helmholtz equation using the separation of variable methods in spherical coordinate system. These functions are introduced in this section.

2.0.1 Bessel Functions

There are two types of Bessel functions, Ordinary and Spherical.

Ordinary Bessel Functions

The differential Equation of the type given below is called Bessel's differential Equation [27].

$$r^2 R'' + r R' + [r^2 - n^2] R = 0 \quad (2.1)$$

where $\frac{\partial}{\partial r}(\frac{\partial}{\partial r}R) = R''$, $\frac{\partial}{\partial r}R = R'$, $-\infty \leq n \leq \infty$, r is the radial distance of a point from the reference point and R is the solution of the equation with respect to the variable r . The particular solution to the above differential equation is given by Bessel's function of the first kind $J_n(r)$, the second kind $Y_n(r)$ and the Hankel function $H_n(r)$ [22]. These functions are plotted in the [22].

The Hankel function in terms of the Bessel functions of the first kind and the second kind is

$$H_n^1(r) = J_n(r) + iY_n(r) \quad (2.2)$$

$$H_n^2(r) = J_n(r) - iY_n(r) \quad (2.3)$$

Where i is the imaginary unit, n is the order, $H_n^1(r)$ and $H_n^2(r)$ are Hankel functions of the first kind and second kind respectively.

Spherical Bessel Functions

Solution to the equation of type given below are called spherical Bessel functions.

$$r^2 R'' + 2r R' + [k^2 r^2 - n(n+1)] R = 0 \quad (2.4)$$

Particular solution to the above differential equation is given by spherical Bessel's function of the first kind $j_n(kr)$, the second kind $y_n(kr)$ and the Hankel function $h_n(kr)$ [22] [39]. The relationship between the ordinary and spherical Bessel functions is given by following expressions [22] [40].

$$j_n(kr) = \sqrt{\frac{1}{2} \frac{\pi}{r}} J_{(n+\frac{1}{2})}(kr) \quad (2.5)$$

$$y_n(kr) = \sqrt{\frac{1}{2} \frac{\pi}{r}} Y_{(n+\frac{1}{2})}(kr) \quad (2.6)$$

$$h_n^1(kr) = j_n(kr) + iy_n(kr) = \sqrt{\frac{1}{2} \frac{\pi}{kr}} H_{(n+\frac{1}{2})}^1(kr) \quad (2.7)$$

$$h_n^2(kr) = j_n(kr) - iy_n(kr) = \sqrt{\frac{1}{2} \frac{\pi}{r}} H_{(n+\frac{1}{2})}^2(kr) \quad (2.8)$$

2.0.2 Legendre Functions and Polynomials

Legendre Functions Legendre functions are the solutions of the ordinary Legendre differential equation which is given by [23]

$$(1 - x^2) \frac{\partial^2 y}{\partial x^2} + 2x \frac{\partial y}{\partial x} + n(n+1)y = 0 \quad (2.9)$$

Solution to above Eqn. is $P_n(x)$ which is known as Legendre functions given

$$y(x) = AP_n(x) + BP_n(-x) \quad (2.10)$$

$$P_n(x) = \frac{1}{2^n n!} \frac{\partial^n}{\partial x^n} [(x^2 - 1)^n] \quad (2.11)$$

where n is the order, m is the degree and $-1 < x < 1$.

$$P_n(-x) = P_n(x)$$

Associated Legendre Polynomials

The following equation is referred to as the associated Legendre differential equation [41].

$$(1 - x^2) \frac{\partial^2 y}{\partial x^2} + 2x \frac{\partial y}{\partial x} + [n(n+1) - \frac{m^2}{1-x^2}]y = 0 \quad (2.12)$$

Solutions are the associated Legendre functions $P_n^m(x)$ and $Q_n^m(x)$ of the first kind and the second kind respectively.

$$y(x) = AP_n^m(x) + BQ_n^m(x) \quad (2.13)$$

Where

$$P_n^m(x) = (-1)^m \frac{(1-x^2)^{(m/2)}}{2^n n!} \frac{d^{m+n}}{dx^{m+n}} [(x^2 - 1)^n] \quad (2.14)$$

and

$$Q_n^m(x) = (-1)^m (1-x^2) \frac{d^m Q_n(x)}{dx^m} \quad (2.15)$$

Any function $f(\theta)$ defined in the interval $0 \leq \theta \leq \pi$ can be represented by series of Legendre Polynomials as follows [23].

$$f(\theta) = \sum_{n=0}^{\infty} a_n P_n(\cos(\theta)) \quad (2.16)$$

2.0.3 Spherical Harmonics

From [11] [40], the solutions of the Helmholtz equation in the radial direction are combined in spherical harmonics. It contains associated legendre polynomials and complex exponential function.

$$Y_n^m(\theta, \phi) = (-1)^m \sqrt{\frac{2n+1}{4\pi} \frac{(n-|m|)!}{(n+|m|)!}} P_n^{|m|}(\cos(\theta)) e^{im\phi} \quad (2.17)$$

Where θ and ϕ are the angles in spherical coordinate system, n , m are order and degree respectively. $n(0, \infty)$, $m(-n, n)$.

BIBLIOGRAPHY

- [1] Yoshida, K.-i., “Applications of fast multipole method to boundary integral equation method,” Kyoto: Kyoto University (2001).
- [2] Taflove, A. and Hagness, S. C., “Computational electrodynamics,” (2000).
- [3] Costabel, M., “Principles of boundary element methods,” *Computer Physics Reports* 6(1), 243–274 (1987).
- [4] Morse, P. M., [Theoretical acoustics], Princeton University Press (1986).
- [5] Greengard, L. and Rokhlin, V., “A fast algorithm for particle simulations,” *Journal of Computational Physics* 135(2), 280–292 (1997).
- [6] Barnes, J. and Hut, P., “A hierarchical $O(n \log n)$ force-calculation algorithm,” (1986).
- [7] Greengard, L., “The numerical solution of the n -body problem,” *Computers in physics* 4(2), 142–152 (1990).
- [8] Wikipedia, “ N -body problem — wikipedia, the free encyclopedia,” (2014). [Online; accessed 13-December-2014].
- [9] Darve, E., “The fast multipole method: numerical implementation,” *Journal of Computational Physics* 160(1), 195–240 (2000).
- [10] Chen, Z., “New approach to a class of matrices,” in [FCS], 135–140 (2006).
- [11] Gumerov, N. A. and Duraiswami, R., [Fast multipole methods for the Helmholtz equation in three dimensions], Elsevier (2005).
- [12] Greengard, L., [The rapid evaluation of potential fields in particle systems], MIT press (1988).
- [13] Carrier, J., Greengard, L., and Rokhlin, V., “A fast adaptive multipole algorithm for particle simulations,” *SIAM Journal on Scientific and Statistical Computing* 9(4), 669–686 (1988).

- [14] Rokhlin, V., “Rapid solution of integral equations of scattering theory in two dimensions,” *Journal of Computational Physics* 86(2), 414–439 (1990).
- [15] Engheta, N., Murphy, W. D., Rokhlin, V., and Vassiliou, M. S., “The fast multipole method (fmm) for electromagnetic scattering problems,” *Antennas and Propagation, IEEE Transactions on* 40(6), 634–641 (1992).
- [16] Cheng, H., Greengard, L., and Rokhlin, V., “A fast adaptive multipole algorithm in three dimensions,” *Journal of Computational Physics* 155(2), 468–498 (1999).
- [17] Ergül, O. and Karaosmanoglu, B., “Using multiple-precision arithmetic to prevent low-frequency breakdowns in the diagonalization of the greens function,” Session 4A11 SC1: Advanced Numerical Techniques in Computational Electromagnetics , 1848 (2014).
- [18] Darrigrand, E., “Coupling of fast multipole method and microlocal discretization for the 3-d helmholtz equation,” *Journal of Computational Physics* 181(1), 126–154 (2002).
- [19] Xu, Y.-L., “Fast evaluation of gaunt coefficients: recursive approach,” *Journal of computational and applied mathematics* 85(1), 53–65 (1997).
- [20] Wikipedia, “Helmholtz equation — wikipedia, the free encyclopedia,” (2014). [Online; accessed 13-December-2014].
- [21] Erdélyi, A. and Bateman, H., “Tables of integral transforms,” (1954).
- [22] Abramowitz, M., Stegun, I. A., et al., [Handbook of mathematical functions], vol. 1, Dover New York (1972).
- [23] Balanis, C. A., [Advanced engineering electromagnetics], vol. 20, Wiley New York (1989).
- [24] Weisstein, E. W., “Delta function,” From MathWorld—A Wolfram Web Resource. <http://mathworld.wolfram.com/DeltaFunction.html> (2005).
- [25] Wikipedia, “Dirac delta function — wikipedia, the free encyclopedia,” (2014). [Online; accessed 13-December-2014].
- [26] Weisstein, E. W., “Bessel function of the first kind, from mathworld—a wolfram web resource,” (2006).
- [27] Wikipedia, “Bessel function — wikipedia, the free encyclopedia,” (2014). [Online; accessed 13-December-2014].
- [28] Wikipedia, “Wronskian — wikipedia, the free encyclopedia,” (2014). [Online; accessed 13-December-2014].
- [29] Spivack, O. R., “May 11, 2012,” (2012).

- [30] Pierce, A. D. et al., [Acoustics: an introduction to its physical principles and applications], McGraw-Hill New York (1981).
- [31] Beatson, R. and Greengard, L., “A short course on fast multipole methods,” Wavelets, multilevel methods and elliptic PDEs 1, 1–37 (1997).
- [32] Coifman, R., Rokhlin, V., and Wandzura, S., “The fast multipole method for the wave equation: A pedestrian prescription,” Antennas and Propagation Magazine, IEEE 35(3), 7–12 (1993).
- [33] Anderson, C. R., “An implementation of the fast multipole method without multipoles,” SIAM Journal on Scientific and Statistical Computing 13(4), 923–947 (1992).
- [34] Chartier, P., Darrigrand, E., and Faou, E., “A regular fast multipole method for geometric numerical integrations of hamiltonian systems,” BIT Numerical Mathematics 50(1), 23–40 (2010).
- [35] Gumerov, N. A. and Duraiswami, R., “Fast, exact, and stable computation of multipole translation and rotation coefficients for the 3-d helmholtz equation,” (2001).
- [36] Song, J., Lu, C.-C., and Chew, W. C., “Multilevel fast multipole algorithm for electromagnetic scattering by large complex objects,” Antennas and Propagation, IEEE Transactions on 45(10), 1488–1493 (1997).
- [37] Wikipedia, “Bessel function — wikipedia, the free encyclopedia,” (2015).
- [38] Umashankar, K. and Taflov, A., [Computational electromagnetics], Artech House (1993).
- [39] NEW, W., “Encyclopedia spherical bessel function,”
- [40] Greengard, L., Huang, J., Rokhlin, V., and Wandzura, S., “Accelerating fast multipole methods for the helmholtz equation at low frequencies,” Computational Science & Engineering, IEEE 5(3), 32–38 (1998).
- [41] Wikipedia, “Associated legendre polynomials — wikipedia, the free encyclopedia,” (2014). [Online; accessed 13-December-2014].

Biography

Nita Nagdewate was born on January 20, 1985 in Nagpur, India. She earned her bachelor's degree in Electrical Engineering from Government College of Engineering, Chandrapur, India. She began her studies at the University of Massachusetts Lowell for Fall 2012 in the Electrical and Computer Engineering Department. In Spring 2013, she joined the Center for Advanced Computation and Telecommunications. She worked as a research member under the guidance of Professor Charles Thompson and Professor Kavitha Chandra. Her research interests are in the fields of Acoustics, Electromagnetics, Astronomy, and Computational Modeling.